Journal of Integrative Neuroscience

J. Integr. Neurosci. **2026**; 25(11): 52481
https://doi.org/10.31083/JIN52481

Original Research

Chronic Sleep Deprivation-Induced Anxiety-Like Behaviors Correlate With Altered Peripheral S100A10+ Immune Cells and Hippocampal Metabolic Dysregulation

Ruifang Hua[1,†], Zhaoteng Hao[1,†], Xiaohang Sheng[2], Qilin Han[1], Zhaorui Liu[1], Peiyang Fu[1], Yunwei Lou[1,*], Hui Wang[1,*]

[1]Henan International Joint Laboratory of Immunology and Model Animals, Henan Collaborative Innovation Center of Molecular Diagnosis and Laboratory Medicine, School of Medical Technology, Xinxiang Medical University, 453003 Xinxiang, Henan, China
[2]School of Basic Medical Sciences, Xinxiang Medical University, 453003 Xinxiang, Henan, China
*Correspondence: ylou@hamu.edu.cn (Yunwei Lou); wanghui@hamu.edu.cn (Hui Wang)
[†]These authors contributed equally.

Academic Editors: Mary Jasmin Ang and Bettina Platt
Submitted: 1 April 2026 Revised: 29 July 2026 Accepted: 5 August 2026 Published: 18 November 2026

Abstract

Objective: To characterize biological alterations associated with chronic sleep deprivation (CSD)-related anxiety-like behaviors in mice and to explore the parallel association between peripheral immunity and central metabolism. **Methods:** A mouse model of CSD was established by subjecting mice to 7 days of sleep deprivation. Anxiety-like behaviors were evaluated using the open field test (OFT) and elevated plus maze (EPM) test. Peripheral blood immune cell subsets and S100A10 levels were analyzed using flow cytometry. Blood-brain barrier (BBB) integrity and inflammatory levels in peripheral blood and hippocampal tissues were assessed through immunofluorescence staining, enzyme-linked immunosorbent assay, and quantitative real-time polymerase chain reaction (qPCR). Hippocampal metabolic profiles were characterized using untargeted metabolomics. Intrinsic interactions among behavioral, immune, and metabolic indices were evaluated through correlation analysis. The functional pathways associated with the differential metabolites were determined using the Kyoto Encyclopedia of Genes and Genomes (KEGG) pathway enrichment analysis. **Results:** CSD mice exhibited typical anxiety-like behaviors, characterized by reduced time spent in the central area in the OFT and fewer entries into that area, as well as increased latency to enter the open arms in the EPM test. At the peripheral immune level, CSD did not alter the proportions of total T cells or total monocytes. However, the proportion of proinflammatory Ly6C$^+$ high monocytes increased, whereas that of anti-inflammatory Ly6C$^+$ low monocytes decreased. CSD disrupted the BBB, promoted microglial activation, and elevated proinflammatory cytokine concentrations in the peripheral blood and hippocampal tissue. Furthermore, CSD upregulated S100A10 expression in CD45$^+$ leukocytes, CD8$^+$ T cells, and total monocytes. At the hippocampal metabolome level, CSD induced 157 differential metabolites. The levels of metabolites including ginsenoyne K were significantly upregulated, while those of metabolites such as phosphatidylinositol were downregulated. Additionally, multiple metabolites were associated with core anxiety-related behavioral parameters. KEGG enrichment analysis revealed that differential metabolites were primarily enriched in neurofunction-related pathways, including the cAMP-signaling pathway and glutathione metabolism. Correlation analysis further unveiled that the proportion of peripheral T cells, the balance between monocyte subsets, S100A10 levels in total monocytes, and key hippocampal metabolites were closely associated with anxiety-like behaviors. **Conclusion:** CSD induces anxiety-like behaviors in mice, it alters the distribution of peripheral monocyte subsets, upregulates S100A10 levels in specific immune cells, and remodels hippocampal metabolism. Moreover, CSD disrupts BBB integrity and activates microglia in the hippocampus.

Keywords: sleep deprivation; anxiety; monocytes; S100A10; hippocampus

1. Introduction

Anxiety disorders are one of the most prevalent mental health conditions worldwide and are considered a major public health concern [1,2]. According to the 2021 Global Burden of Disease (GBD) estimates, anxiety disorders affected 359.2 million people worldwide, with an age-standardized prevalence of 4.4%, imposing enormous societal burdens [3]. Epidemiological studies have reported that the prevalence of anxiety disorders positively correlates with socioeconomic development and urbanization, which is consistent with the current severe situation [4]. Characterized by a chronic course and high lifetime prevalence, anxiety disorders severely impair the quality of life and social functioning of patients. Furthermore, they are typically associated with somatic symptoms, including sleep disturbances and palpitations [2].

Insomnia plays several crucial roles in mood disorders, serving as a risk factor, a comorbid condition, and a transdiagnostic core symptom. Furthermore, insomnia is considered a marker of impaired neuroplasticity and contributes to the dysregulation of several neurobiological

Copyright: © 2026 The Author(s). Published by IMR Press.
This is an open access article under the CC BY 4.0 license.

Publisher's Note: IMR Press stays neutral with regard to jurisdictional claims in published maps and institutional affiliations.

mechanisms associated with mental disorders [5]. Chronic sleep deprivation (CSD) is a prevalent type of sleep disturbance in modern society. Clinical and experimental studies suggest a clear bidirectional causal relationship between CSD and anxiety disorders. Sleep deprivation may hamper an individual's ability to regulate emotions and enhance stress sensitivity, thus increasing the risk of anxiety disorders. Moreover, CSD may induce executive dysfunction to aggravate emotional disturbances [6,7]. Conversely, patients with anxiety-related insomnia often enter into a vicious cycle of "insomnia–anxiety", which further exacerbates sleep disorders [8,9,10]. A longitudinal study on women reported that persistent sleep difficulties are associated with the onset, recurrence, and maintenance of anxiety and depressive disorders [9,11]. A 20-year follow-up study in a Swiss population demonstrated that insomnia is prospectively associated with the development of depressive episodes [12]. Increasing evidence also suggests that both sleep disturbances and psychological disorders are closely associated with dysregulation of the immune and neuroendocrine systems [13,14,15].

The peripheral immune system serves as a core hub for sensing and responding to stress stimuli. The dysfunction of the peripheral immune system, mediated by the neuro–immune–endocrine interaction network, plays an indispensable role in stress-related emotional disorders [16]. Monocytes are key effector cells of the peripheral immune system and can be classified into proinflammatory (Ly6C$^+$ high) and anti-inflammatory (Ly6C$^+$ low) subsets according to their Ly6C surface expression. The dynamic balance between these two subsets regulates the inflammatory status of the peripheral immune microenvironment [17]. Ly6C$^+$ high monocytes serve as precursors of Ly6C$^+$ low monocytes and dynamically respond to changes in the microenvironment. Initially, they exhibit a proinflammatory phenotype to remove necrotic tissues and pathogens before differentiating into an anti-inflammatory phenotype to restore tissue homeostasis [18]. This balance is mainly co-regulated by sympathetic nerve signals and the hypothalamic–pituitary–adrenal axis [16], indicating a close association with stress and stress-induced mood disorders. Previous studies have reported that chronic stress stimulates the proliferation of bone marrow hematopoietic progenitor cells, induces the mobilization of Ly6C$^+$ high monocytes into circulation, and suppresses the function of Ly6C$^+$ low monocytes, leading to an imbalance in monocyte subsets [16]. Ly6C$^+$ high monocytes can bind to mucosal addressin cell adhesion molecule-1 on cerebral vascular endothelial cells via surface α4β7 integrin, promoting neutrophil recruitment into the brain and increasing the production of interleukin-1β (IL-1β) and C-C motif chemokine ligand 2 (CCL2), ultimately contributing to anxiety-like behaviors [19]. During psychological stress, stress-induced IL-6 promotes a proinflammatory priming phenotype in Ly6C$^+$ high monocytes. After entering the brain, these cells amplify neuroinflammation by enhancing IL-1β signaling, leading to anxiety and social avoidance behaviors [20].

S100A10, also known as P11, is a calcium-binding protein that is involved in immune cell activation, inflammatory factor production, and central emotional regulation [21]. Emerging evidence suggests that S100A10 expression in peripheral immune cells may serve as a potential biomarker for depression. In clinical studies, S100A10 expression was upregulated in circulating CD4$^+$ T cells from patients with major depressive disorder (MDD). Moreover, S100A10 levels in monocytes, CD4$^+$ T cells, and CD8$^+$ T cells were negatively correlated with anhedonia severity [22]. Ketamine treatment markedly downregulated p11 expression in CD4$^+$ T cells and CD8$^+$ T cells [23]. Two weeks of citalopram treatment also downregulated p11 expression in natural killer (NK) cells and monocytes, with the magnitude of reduction correlating with improvements in clinical symptoms of depression, as determined using the Montgomery–Åsberg Depression Rating Scale (MADRS) after 8-week treatment [24]. In patients with Parkinson's disease (PD), S100A10 mRNA and protein levels were markedly reduced in dopaminergic neurons of the substantia nigra, but they increased in peripheral monocytes, NK cells, and CD8$^+$ T cells, where it positively correlated with PD disease severity. Furthermore, S100A10 expression in these three immune subsets effectively discriminated healthy subjects from PD patients with comorbid depression [25]. Collectively, these findings suggest that peripheral immune cell-derived S100A10 may represent a potential blood biomarker for anxiety and other affective disorders.

The hippocampus is a critical brain region of the central nervous system (CNS) that regulates emotional homeostasis. The functional integrity of the hippocampus is important for emotion regulation [26,27]. However, stress can disrupt the integrity of the hippocampal mitochondrial metabolic network and neuronal connectivity [28]. As a major process in hippocampus-dependent memory consolidation and metabolic repair [29,30], sleep deprivation can induce hippocampal microglial activation and increase inflammatory factors, thereby exacerbating neuronal damage [31]. Furthermore, recent preclinical evidence highlights that sleep disturbances profoundly impair hippocampal neuroplasticity, contributing to cognitive and emotional dysfunction [32]. Nevertheless, the role of CSD in the hippocampal metabolome and its association with peripheral immunity and anxiety-like behaviors is yet to be reported.

Based on current evidence, this study sought to elucidate the biological alterations associated with CSD-induced anxiety-like behaviors and the parallel association between peripheral immunity and central metabolism. We established a CSD mouse model using the modified multiple-platform water environment method. Anxiety-like behaviors were determined by behavioral tests and peripheral blood leukocyte subsets. Additionally, S100A10 ex-

pression was assessed by flow cytometry, and hippocampal metabolic remodeling was characterized by untargeted metabolomics. Through correlation analysis, we aimed to explore key biological links among peripheral immunity, central metabolism, and CSD-induced anxiety-like behaviors, which may provide candidate clues and potential biomarkers for interventions targeting sleep disturbance-related emotional disorders.

2. Materials and Methods

2.1 Animals

8-week-old male C57BL/6J mice (n = 33) were purchased from Beijing Vital River Laboratory Animal Technology Co., Ltd. (Beijing, China). All mice were housed in a specific pathogen-free (SPF) animal facility under controlled environmental conditions: a 12 h light/12 h dark cycle (lights on: 8:00–20:00), temperature maintained at 23 ± 2 °C, and relative humidity at 55 ± 5%. Mice had *ad libitum* access to food and water. These mice were assigned to three independent cohorts, and no animals were reused between experiments. Cohort 1 (Control, n = 7; CSD, n = 6) was used for flow cytometry and untargeted metabolomics. Cohort 2 (Control, n = 4; CSD, n = 4) was used for immunofluorescence. Cohort 3 (Control, n = 7; CSD, n = 5) was used for ELISA and qPCR. Before tissue collection for molecular biological experiments, the mice were euthanized via isoflurane inhalation, followed by cervical dislocation. The hippocampal tissues were rapidly dissected once spontaneous breathing ceased, and then all limb reflexes were completely abolished. The study was carried out in accordance with the ARRIVE guidelines (**Supplementary Material-ARRIVE checklist**).

2.2 Treatment of Sleep Deprivation

All mice were allowed to acclimate to the housing environment for 7 days. The mice were randomly assigned to two groups: the Control group (Control) and the CSD group. A modified Multiple Platform Method (mMPM) was used. The sleep deprivation apparatus consisted of a rectangular water tank (dimensions: 32 cm × 22 cm × 16 cm), in which 9 acrylic cylinders (diameter: 3 cm) were vertically placed in a 3 × 3 grid. The distance between adjacent cylinders was 5 cm. The top of each cylinder (i.e., the platform for mice to stand on) was approximately 1 cm above the water surface in the tank, and tap water was added to the tank to a height of 10 cm. Mice in the CSD group could move between the cylinders. Mice in the Control group were housed in the same environment with free movement on a large platform (20 cm × 20 cm).

The sleep deprivation protocol consisted of 20 h of sleep deprivation per day, from 16:00 to 12:00 the following day, followed by a 4-h recovery period (12:00–16:00) during which the mice were allowed free movement. This regimen was maintained for 7 consecutive days. Throughout the experimental period, the mice had *ad libitum* access to food and water. The water in the tank was replaced daily to maintain a clean and hygienic environment.

2.3 Behavioral Tests

All behavioral tests were performed in a sound-attenuated and light-controlled room with a light intensity of 50 ± 5 lux. All tests were conducted between 09:00 and 17:00. The mice were acclimated to the testing room for 30 minutes before the test. The open field test and elevated plus maze were performed on the same day, with a 6-hour interval between the two tests for each mouse. After testing each mouse, the apparatus was cleaned with 75% ethanol and air-dried before the next mouse was tested. Both behavioral testing and data analysis were performed using the SuperMaze Behavioral Analysis System (Version 3.0, Shanghai Xinruan Information Technology Co., Ltd., China).

2.3.1 Open Field Test (OFT)

The OFT was used to evaluate spontaneous locomotor activity and anxiety-like behavior in mice. The OFT arena (40 cm × 40 cm × 40 cm) was constructed from white matte acrylic. A high-definition camera was fixed 100 cm directly above the center of the arena and connected to the SuperMaze Behavioral Analysis System (Version 3.0, Shanghai Xinruan Information Technology Co., Ltd., China), which automatically recorded and analyzed the mouse's movement trajectory and related parameters.

Each mouse was gently placed in the central area with a consistent orientation maintained during placement. The system recorded and analyzed the mouse's behavior over a 10-minute period. After testing, the mouse was returned to its home cage, and the inner walls and floor of the arena were thoroughly cleaned with 75% ethanol; the arena was air-dried before testing the next mouse. The central zone of the OFT arena was defined as a 20 cm × 20 cm area (occupying 1/4 of the total arena area), and the area outside the central zone was designated as the peripheral zone. The core parameters analyzed in this experiment included: total distance traveled, proportion of time spent in the central zone, and number of entries into the central zone.

2.3.2 Elevated Plus Maze (EPM)

The EPM apparatus was made of white acrylic and consisted of four arms. It included 2 open arms (length × width: 35 cm × 5 cm, no sidewalls), 2 closed arms (length × width: 35 cm × 5 cm, with 15 ± 0.5 cm high sidewalls), and a central platform (5 cm × 5 cm). The entire maze was elevated 80 cm above the ground.

At the start of the experiment, each mouse was gently placed on the central platform with its head facing one of the open arms (a consistent orientation was maintained for all mice). The mouse was then allowed to explore freely for 6 minutes. All maze arms and the central platform were wiped clean with 75% ethanol to completely remove residual odors before testing the next mouse. For experimen-

tal data analysis, the last 5 minutes of the free exploration period were analyzed. The core parameters analyzed included: average speed, latency to first entry into the open arms, and times of head exploration.

2.4 Flow Cytometric Detection of Peripheral Blood Cell Proportions and S100A10 Fluorescence Intensity

2.4.1 Sample Collection

The experimental mice were briefly anesthetized by using the open-drop method for retro-orbital blood collection. Briefly, a cotton ball soaked with 0.5 mL isoflurane (Cat. No. R510-22-10, RWD Life Science Co., Ltd., Shenzhen, China) was placed in a 500-mL induction chamber. The mouse was introduced into the chamber and monitored until the loss of righting reflex and the absence of toe-pinch response (typically 10–20 s), indicating adequate anesthesia. The body temperature was maintained at 37 °C using a heating pad throughout the procedure. Immediately thereafter, 200 µL of blood was collected from the inner canthus via a heparinized capillary tube and transferred into a 1.5 mL microcentrifuge tube containing ethylenediaminetetraacetic acid (EDTA)-K2 (Cat. No. HR10013; Lengrui, Nantong, China). The total duration of anesthesia was limited to 1–2 min. The samples were processed within 30 min. At the experimental endpoint, the mice were euthanized via cervical dislocation, with death confirmed by cessation of breathing and the absence of corneal reflex.

2.4.2 Staining of Cell Surface Markers

100 µL of the mixed anticoagulated blood was transferred to a new RNase-free 1.5 mL microcentrifuge tube. Subsequently, 50 µL of fluorescein-conjugated antibody mixture (see Table 1) was added to each tube. The antibody mixture was prepared with PBS containing 1% fetal bovine serum (Cat. No. 10099-141; Gibco, Grand Island, NY, USA) at a dilution ratio of 1:300. After gentle pipetting to mix, the samples were incubated at 4 °C in the dark for 20 minutes to complete cell surface staining.

Table 1. Antibodies for flow cytometric analysis.

Antibody target	Fluorescent label	Manufacturer	Catalog number
CD45	V450	Invitrogen, Eugene, OR, USA	48-0451-82
CD4	PE	BioLegend, San Diego, CA, USA	100512
CD8	APC-Cy7	BD Biosciences, San Jose, CA, USA	557654
CD115	PE-Cy7	BioLegend, USA	135523
CD11b	APC	BioLegend, USA	101212
Ly6C	PE-Cy5	BioLegend, USA	128012

2.4.3 Red Blood Cell Lysis

After completion of cell surface staining, 1 mL of red blood cell lysis buffer (Catalog No.: R1010, Solarbio, Beijing, China) was added to each sample, followed by lysis at 4 °C in the dark for 10 minutes. During lysis, the samples were inverted and mixed twice to ensure thorough lysis. After lysis, centrifugation was performed at 2700 rpm at 4 °C for 6 minutes. The supernatant was discarded, and the completeness of lysis was checked. Subsequently, 1 mL of 0.01 M PBS was added to each sample tube for rinsing, followed by centrifugation at 2700 rpm at 4 °C for 6 minutes.

2.4.4 Fixation and Permeabilization

100 µL of BD Cytofix/Cytoperm™ fixation and permeabilization solution (Catalog No.: 51-2090KZ, BD Biosciences, USA) was added to the cell pellet of each sample. After pipetting to mix thoroughly, the samples were transferred to a 96-well plate and incubated at 4 °C in the dark for 30 minutes. Then, centrifugation was performed at 1800 rpm at 4 °C for 6 minutes. After discarding the supernatant, 200 µL of 1× BD Perm/Wash™ buffer (Catalog No.: 51-2091KZ) was added to each well for rinsing, followed by centrifugation at 1800 rpm at 4 °C for 6 minutes. This washing step was repeated twice.

2.4.5 S100A10 Staining

50 µL of diluted S100A10 antibody (diluted in 1× Perm/Wash buffer at 1:100; Cat. No. 11250-1-AP; Proteintech, Wuhan, China) was added to the cell pellet in each well. The samples were incubated at 4 °C in the dark for 30 minutes. After rinsing twice with 1× Perm/Wash buffer, 50 µL of Goat anti-Rabbit IgG (H+L) Cross-Adsorbed Secondary Antibody, Alexa Fluor™ 488 (A-11008, Invitrogen; prepared in 1× Perm/Wash buffer at 1:800) was added to each well, followed by incubation at 4 °C in the dark for 30 minutes. Each well was then rinsed twice with 200 µL of 1× BD Perm/Wash™ buffer.

2.4.6 Flow Cytometry Detection and Data Analysis

Each sample was resuspended in 300 µL of 1× BD Perm/Wash™ buffer, then filtered through a 100-mesh steel sieve and transferred to a flow cytometry tube. Data were acquired using an Attune NxT flow cytometer (Model No. Attune NxT; Thermo Fisher Scientific, Waltham, MA, USA). At least 1×10^5 nucleated cells were collected per sample. The detection results were analyzed using FlowJo software (Version 10.8, BD Biosciences, San Jose, CA, USA). Fluorescence compensation was performed using the automated compensation algorithm in FlowJo software (Version 10.8) based on the fully stained samples. The gating strategy was as follows: nucleated cells were selected based on forward scatter (FSC) and side scatter (SSC); leukocytes were gated as $CD45^+$ cells; specific cell subsets were further identified: $CD4^+$ T cells ($CD45^+CD4^+CD8^-$), $CD8^+$ T cells ($CD45^+CD8^+CD4^-$),

and monocytes ($CD45^+CD11b^+CD115^+Ly6C^{+/-}$). For S100A10 gating, the negative control (NC) shown in the histograms was a sample stained only with surface markers without S100A10 antibody, which was used to establish the positivity gate and exclude background autofluorescence. The mean fluorescence intensity (MFI) of S100A10 in each cell subset was quantified.

2.5 Enzyme-Linked Immunosorbent Assay (ELISA)

After 3 h of the behavioral tests, blood samples were collected into 1.5 mL microcentrifuge tubes and allowed to coagulate at room temperature for 30 min, followed by centrifugation at 12,000 rpm for 10 min at 4 °C. The levels of IL-6, IL-1β, and TNF-α in the blood serum were determined using a mouse TNF-α ELISA Kit (Cat. No. KE10002, Proteintech, Wuhan, Hubei, China), a mouse IL-6 ELISA Kit (Cat. No. KE10007, Proteintech, China), and a mouse IL-1β ELISA Kit (Cat. No. KE10003, Proteintech, China). All experimental operations for ELISA were performed in line with the manufacturer's guidelines.

2.6 Immunofluorescence Staining

To evaluate the effects of CSD on hippocampal neuroinflammation and BBB integrity, the experimental mice were intraperitoneally anesthetized with sodium pentobarbital (100 mg/kg; Sigma-Aldrich, St. Louis, MO, USA; Cat. No.: P3761) 3 h after behavioral tests, followed by transcardial perfusion fixation. The brain tissues were post-fixed in 4% paraformaldehyde for 8–12 h. Then, 40 µm-thick coronal brain sections of the hippocampus were prepared using the VT1200S vibratome (Leica Biosystems, Nussloch, Germany). The sections were rinsed thrice with 0.01 M PBS (15 min/wash), then blocked with 0.01 M PBS containing 0.3% Triton X-100 and 10% goat serum at room temperature (RT) for 90 min. After blocking, the sections were incubated with primary antibodies overnight at 4 °C. The primary antibodies used in the study were rabbit anti-Iba1 (Cat. No. 019-19741, 1:1500, Wako Pure Chemical Industries, Ltd., Osaka, Japan) and rabbit anti-ZO-1 (Cat. No. 21773-1-AP, 1:200, Proteintech, China).

After incubation with the primary antibodies, the sections were washed thrice in 0.01 M PBS (15 min/wash) and incubated with secondary antibodies for 2 h at RT in the dark. For secondary antibody incubation, goat anti-rabbit IgG (H+L) conjugated to Alexa Fluor™ 594 (Catalog No. A-11012, dilution 1:1000, Invitrogen, Eugene, OR, USA) was used to label Iba1 and ZO-1. The nuclei were counterstained with 4′,6-Diamidino-2-phenylindole (DAPI, 5 µg/mL, Cat. No. 10236276001, Roche, Basel, Switzerland) for 15 min at RT. Following PBS rinsing, the sections were mounted with 50% glycerol.

Fluorescence images were collected using a Nikon Ti2-E laser-scanning confocal microscope (Nikon Instruments Inc., Tokyo, Japan) equipped with 10× and 20× objectives. The quantitative analysis of the number of Iba1-positive cells and the MFI of ZO-1 was performed using ImageJ (v1.53e, NIH, Bethesda, MD, USA).

2.7 Quantitative Real-Time Polymerase Chain Reaction (qPCR)

After 3 h of behavioral testing, the mice were anesthetized with isoflurane and euthanized by cervical dislocation, and the hippocampal tissues were rapidly dissected on an ice bath. Total RNA was extracted using TRizol reagent (Invitrogen, Carlsbad, CA, USA). The concentration and purity of RNA were quantified with the NanoDrop 1000 spectrophotometer. Subsequently, 1 µg of total RNA was reverse-transcribed into complementary DNA (cDNA) using PrimeScript™ RT Master Mix (Perfect Real Time) (Cat. No. RR036A, Takara Bio, Shiga, Japan), and the obtained cDNA was stored at −20 °C for subsequent analyses.

The qPCR reactions were conducted with TB Green® Premix Ex Taq™ II (Tli RNaseH Plus) (Cat. No. RR820A, Takara Bio) on an ABI 750 FAST qPCR instrument (Applied Biosystems, Foster City, CA, USA). All samples were assayed in triplicate to guarantee experimental accuracy. All primer sequences for qPCR are listed in Table 2. The relative expression of the target genes was calculated using the $2^{-\Delta\Delta Ct}$ method.

2.8 Untargeted Metabolomics Analysis of Hippocampal Tissues

2.8.1 Sample Preparation

After 3 h of behavioral tests, the mice were anesthetized through isoflurane inhalation and euthanized by cervical dislocation, and the hippocampi were rapidly dissected, followed by immediate snap-freezing in liquid nitrogen and storage at −80 °C.

2.8.2 Metabolite Extraction and LC-MS Analysis

The hippocampal tissue (20 mg) was precisely weighed and transferred into a 1.5-mL EP tube. Quality control (QC) samples were prepared by mixing equal volumes of extracts from all individual biological samples. Pre-chilled methanol/water (4:1, v/v) solution was added, and homogenization was performed using a bead mill homogenizer at low temperature. Subsequent steps included vortexing, sonication, centrifugation to collect supernatant, and vacuum freeze-drying to obtain dried metabolite powder.

Dried samples were reconstituted with acetonitrile/water (1:1, v/v), and after centrifugation, the supernatant was subjected to LC-MS analysis. Chromatographic separation was performed using a Waters ACQUITY UPLC HSS T3 column (100 mm × 2.1 mm, 1.8 µm; Waters Technologies (Shanghai) Co., Ltd., Shanghai, China) maintained at 40 °C. The mobile phase consisted of 0.1% formic acid in water (Phase A) and acetonitrile (Phase B), with gradient elution. Mass spectrometry (MS) detection was conducted using the Q-Exactive HF-X mass spectrometer

Table 2. Primer sequences for qPCR.

Gene name	Forward Primer (5′→3′)	Reverse Primer (5′→3′)
Gapdh	CATCACTGCCACCCAGAAGACTG	ATGCCAGTGAGCTTCCCGTTCAG
Il6	CTGCAAGAGACTTCCATCCAGTT	AGGGAAGGCCGTGGTTGT
Il1b	GTCACAAGAAACCATGGCACAT	GCCCATCAGAGGCAAGGA
Tnf	GGCTGCCCCGACTACGT	ACTTTCTCCTGGTATGAGATAGCAAAT
Cd86	TTGTGTGTGTTCTGGAAACGGAG	AACTTAGAGGCTGTGTTGCTGG
Nos2	GTTCTCAGCCCAACAATACAAGA	GTGGACGGGTCGATGTCAC
Arg1	AAGAATGGAAGAGTCAGTGTGG	GGGAGTGTTGATGTCAGTGTG
Mrc1	CTCTGTTCAGCTATTGGACGC	CGGAATTTCTGGGATTCAGCTTC

(Model No. Q-Exactive HF-X; Thermo Fisher Scientific, Waltham, MA, USA) equipped with an electrospray ionization (ESI) source, performing full scan (m/z 70–1050) and data-dependent secondary MS acquisition (DDA MS/MS) in both the positive and negative ion modes.

2.8.3 Data Processing and Statistical Analysis

Raw data were processed using Compound Discoverer software (Version 3.3, Thermo Fisher Scientific, Waltham, MA, USA) for peak extraction, alignment, and compound identification, with databases including mzCloud, mzVault, and HMDB. All metabolic datasets were normalized to corresponding tissue weights before statistical analysis. Differential metabolites were selected based on nominal $p < 0.05$ and fold change (FC $\geq$1.2 or FC $\leq$1/1.2).

Volcano plots were used to visualize the screening results, with $-\log10$(*p*-value) as the Y-axis and log2(FC) as the X-axis. Red and blue dots represented significantly different metabolites meeting the screening criteria, facilitating the visual identification of metabolite distribution patterns.

Functionally relevant metabolites were further investigated by selecting the top 50 significantly differential metabolites with the smallest *p*-values followed by separate differential expression analysis and subsequent correlation analysis. Pathway enrichment analysis of differential metabolites was performed using the Kyoto Encyclopedia of Genes and Genomes (KEGG) database.

2.9 Correlation Analysis

To evaluate linear correlations between paired variables (e.g., behavioral parameters and peripheral immune cell proportions, S100A10 MFI and hippocampal metabolites), the Shapiro–Wilk test was first conducted to test data normality. Pearson correlation analysis was applied to normally distributed datasets, whereas Spearman correlation analysis was adopted for non-normal data. Correlation strength was assessed using correlation coefficients (r) and corresponding *p*-values, and $p < 0.05$ was regarded as statistically significant.

2.10 Statistical Methods

All experimental data were analyzed using GraphPad Prism 8.0.2 software (GraphPad Software, Inc., San Diego, CA, USA). All experimental results were uniformly expressed as the mean ± standard error of the mean (S.E.M.). The sample size (n) represents the number of independent mice in each experimental group. Statistical significance of intergroup differences was determined using a two-tailed unpaired *t*-test. The significance levels were annotated as follows: $*p < 0.05$, $**p < 0.01$, $***p < 0.001$; results with no statistical significance were annotated as n.s. (no significance).

3. Results

3.1 CSD Induces Anxiety-Like Behaviors in Mice

To determine the effects of CSD on the emotional states of mice, a CSD model was established by subjecting mice to 7 consecutive days of sleep deprivation (20 h of sleep deprivation and 4 h of rest per day). On the following day, the OFT and EPM test were performed to evaluate anxiety-like behaviors in mice. After the behavioral tests were conducted, the number of peripheral blood leukocytes was analyzed through flow cytometry, and hippocampal metabolic profiles were characterized through untargeted metabolomics (Fig. 1A).

The OFT results revealed that the CSD mice exhibited a shorter total travel distance, a significantly lower percentage of time spent in the central area, and significantly fewer entries into the central area than the control mice (Fig. 1B,C). However, no differences were observed in the average locomotor speed of either the central or peripheral zones (**Supplementary Fig. 1A,B**). In the EPM test, the CSD mice exhibited a lower average moving speed, significantly prolonged latency to enter the open arms, and significantly fewer head-dipping explorations than the control mice (Fig. 1D,E). Collectively, these findings demonstrate that CSD treatment induces anxiety-like behaviors in mice.

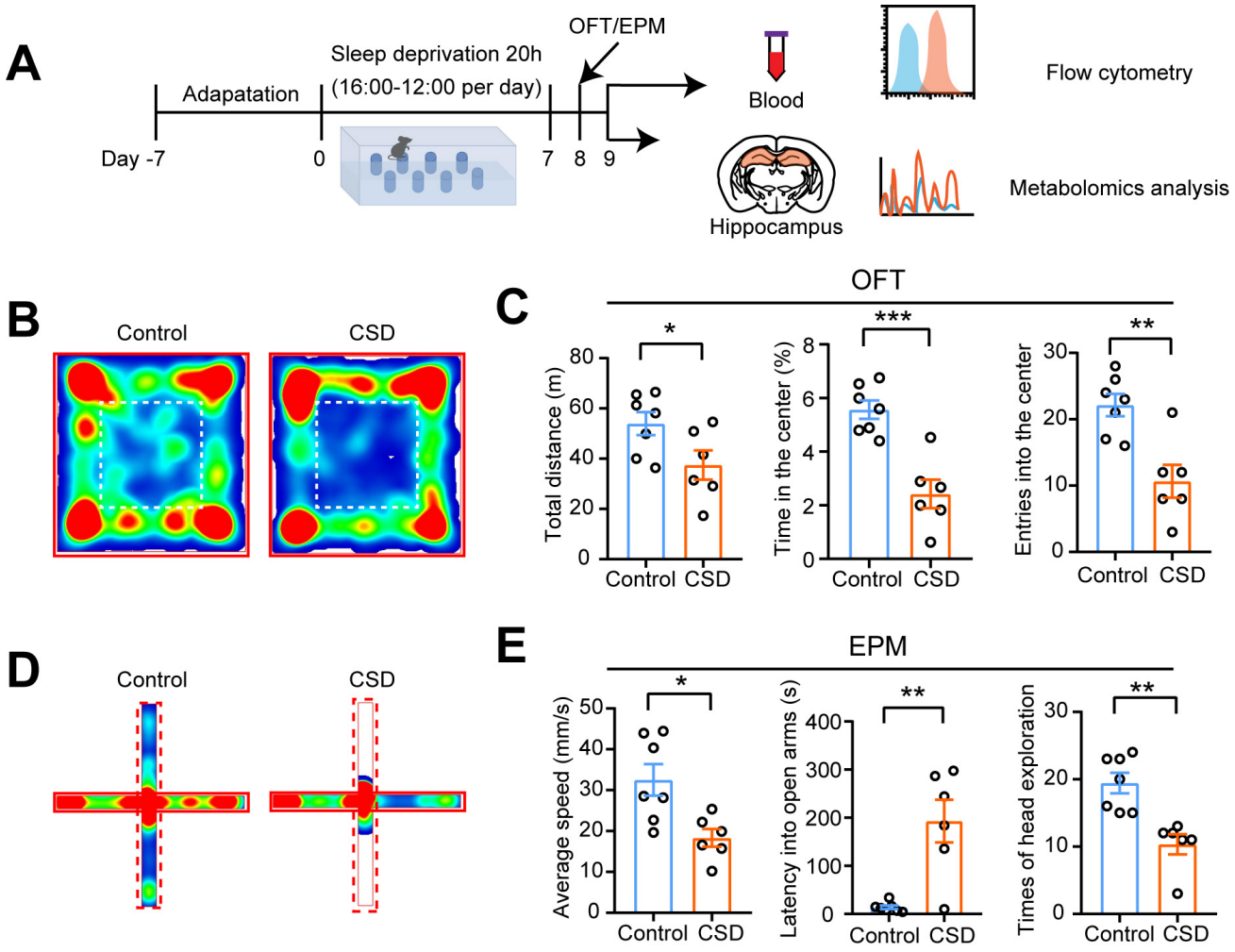


Fig. 1. Chronic sleep deprivation (CSD) induces anxiety-like behaviors in mice. (A) Depiction of the experimental flowchart. (B) Representative heatmaps of movement trajectories in the Open Field Test (OFT). Control: mice in the normal sleep group; CSD: mice in the CSD group. The white dashed line marks the boundary of the central area of the open field apparatus. The color intensity of the heatmap indicates the duration of the mice's stay in different areas. (C) Bar graphs depicting a decrease in total distance (left panel), the proportion of time spent in the central area (middle panel), and the number of entries into the central area (right panel) in the OFT. (D) Representative heatmaps of movement trajectories in the Elevated Plus Maze (EPM) test. The red solid lines mark the closed arms, and the red dashed lines mark the open arms. The color intensity of the heatmap reflects the duration of the mice's stay in different arms. (E) Bar graphs depicting the average movement speed (left panel), the latency to first entry into the open arms (middle panel), and times of head exploration (right panel). Control, n = 7; CSD, n = 6. Data are presented as the mean ± S.E.M., two-tailed unpaired *t*-test. *$p < 0.05$, **$p < 0.01$, ***$p < 0.001$.

3.2 CSD Alters the Proportion of Peripheral Blood Monocyte Subsets and S100A10 Levels in Specific Leukocyte Subsets in Mice

3.2.1 CSD Alters Peripheral Blood Monocyte Subset Proportions in Mice

To investigate peripheral immune alterations associated with CSD-induced anxiety-like behaviors, we analyzed the proportions and subset distributions of T cells and monocytes in peripheral blood through flow cytometry. The gating strategies were as follows: First, peripheral blood leukocytes were labeled with $CD45^+$ for initial gating (Fig. 2A). In the $CD45^+$ cell population, T cells were further divided into $CD4^+$ T cells and $CD8^+$ T cells based on $CD4^+$ and $CD8^+$ expression (Fig. 2B). The monocyte population was defined by the double positivity for $CD11b^+$ and $CD115^+$ as markers (Fig. 2C) and subsequently subdivided into two subsets: $Ly6C^+$ high monocytes and $Ly6C^+$ low monocytes, based on Ly6C expression (Fig. 2D). No significant difference was found in the proportions of $CD45^+$ leukocytes, $CD4^+$ T cells, $CD8^+$ T cells, and monocytes in the peripheral blood of the two groups (Fig. 2E–H). However, the proportion of proinflammatory $Ly6C^+$ high monocytes was significantly increased. In contrast, the proportion of anti-inflammatory $Ly6C^+$ low monocytes was sig-

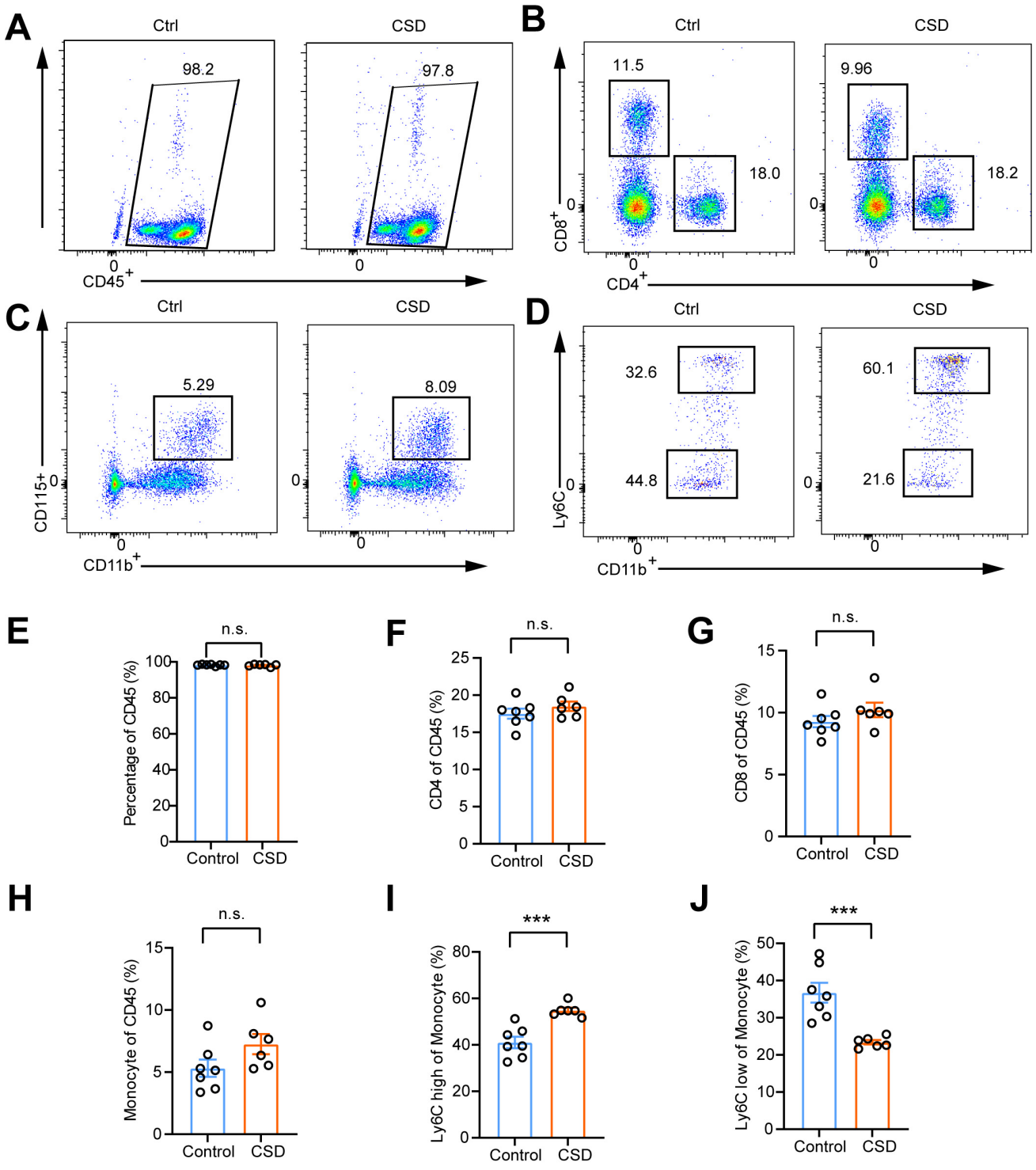


Fig. 2. CSD induces alterations in the percentage of immune cells in peripheral blood in mice. (A–D) Flow cytometry dot plots illustrating the gating strategy for peripheral immune cells. (A) Gating of total $CD45^+$ immune cells; (B) Separation of $CD4^+$ and $CD8^+$ T lymphocyte subsets; (C) Gating of $CD11b^+$ $CD115^+$ monocytes; (D) Subdivision of monocytes into $Ly6C^+$high and $Ly6C^+$low populations. (E–J) Bar graphs quantifying the percentage of each immune subset, including the percentage of $CD45^+$ cells (E), $CD4^+$ T cells of $CD45^+$ (F), $CD8^+$ T cells of $CD45^+$ (G), monocytes of $CD45^+$ (H), $Ly6C^+$high monocytes in total monocytes (I), and $Ly6C^+$low monocytes in total monocytes (J). Control, n = 7; CSD, n = 6. Data are presented as the mean ± S.E.M., two-tailed unpaired *t*-test. ***$p < 0.001$, n.s., no statistical significance.

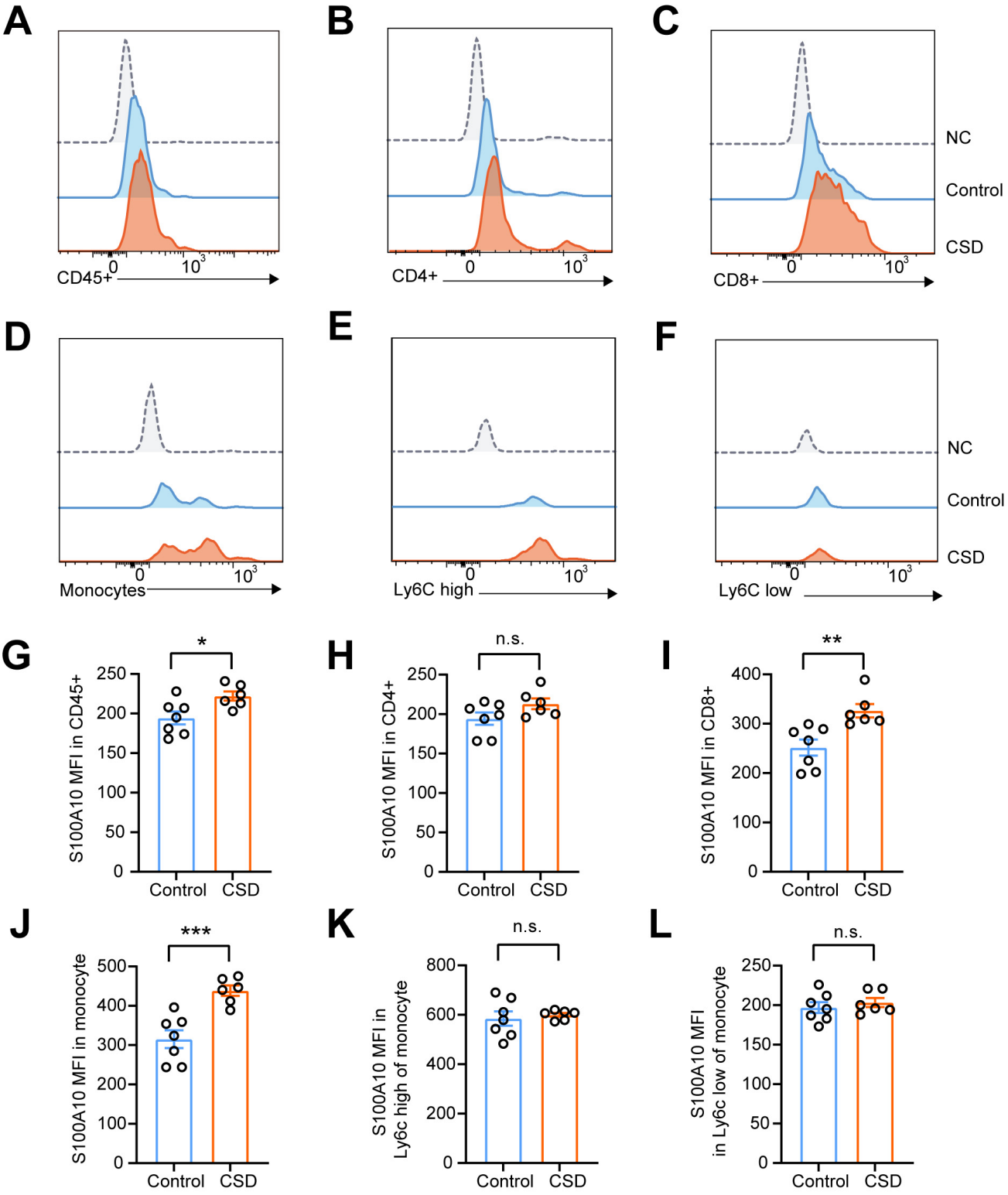


Fig. 3. CSD alters S100A10 expression in peripheral blood immune cells of mice. (A–F) Histograms showing S100A10 levels in peripheral blood CD45$^+$ immune cells (A), CD4$^+$ T cells (B), CD8$^+$ T cells (C), monocytes (D), Ly6C$^+$ high monocytes (E), and Ly6C$^+$ low monocytes (F), measured by flow cytometry. Gray dashed line: negative control (NC); blue curve: control group; orange curve: CSD group. (G–L) Bar graphs displaying S100A10 mean fluorescence intensity (MFI) in CD45$^+$ cells (G), CD4$^+$ T cells (H), CD8$^+$ T cells (I), monocytes (J), Ly6C$^+$ high monocytes (K), and Ly6C$^+$ low monocytes (L). Control, n = 7; CSD, n = 6. Data are presented as the mean ± S.E.M.. and analyzed using a two-tailed unpaired *t*-test. *$p < 0.05$, **$p < 0.01$, ***$p < 0.001$, n.s., no statistical significance.

nificantly decreased in the CSD group compared with the control group (Fig. 2I,J). These results indicate that CSD interferes with peripheral monocyte balance and could be associated with the development of anxiety-like behaviors.

3.2.2 CSD Upregulates S100A10 Levels in Certain Peripheral Blood Leukocyte Subsets

Because S100A10 is a major calcium-binding protein involved in immune activation and the regulation of anxiety-like behaviors, we analyzed the MFI of S100A10 in different peripheral blood leukocyte subsets using flow cytometry (Fig. 3). Representative flow cytometry plots (Fig. 3A–F) revealed differences in S100A10 staining among various cell subsets. Quantitative analysis showed that, compared with the control group, the CSD group showed significantly increased S100A10 levels in CD45+ leukocytes (Fig. 3G), $CD8^+$ T cells (Fig. 3I), and total monocytes (Fig. 3J). Nevertheless, no significant difference in S100A10 levels was observed in CD4+ T cells (Fig. 3H), $Ly6C^+$ high monocytes (Fig. 3K), or $Ly6C^+$ low monocytes (Fig. 3L) between the two groups. These results indicate that CSD selectively upregulates S100A10 levels in $CD8^+$ T cells and monocytes, potentially correlating with anxiety-like behavior.

3.3 Correlation Analysis Among Anxiety-Like Behavior Parameters, Peripheral Immune Indicators, and S100A10 Expression

To further determine the relationship between peripheral immune alterations and anxiety-like behaviors, correlation analysis was performed to evaluate the associations among behavioral parameters from the OFT and EPM tests, peripheral immune cell proportions, and S100A10 expression (Figs. 4,5).

The percentage of time spent in the central zone during the OFT was negatively correlated with the proportions of $CD4^+$ T cells (Fig. 4B), $CD8^+$ T cells (Fig. 4C), and $Ly6C^+$ high monocytes (Fig. 4E), whereas it was positively correlated with the proportion of $Ly6C^+$ low monocytes (Fig. 4F). No significant correlations were observed between the percentage of time spent in the central zone and the proportions of $CD45^+$ cells (Fig. 4A) and total monocytes (Fig. 4D). In addition, the percentage of time spent in the central zone was negatively correlated with the S100A10 levels in total monocytes (Fig. 4J). By contrast, no significant associations were observed between time spent in the central zone and the S100A10 levels in other cell populations (Fig. 4G–I,K,L).

We next analyzed the relationships between the latency to first enter the open arms in the EPM test and the proportions of peripheral immune cells, as well as S100A10 levels in these cells. The latency to enter the open arms was positively correlated with the proportion of $Ly6C^+$ high monocytes (Fig. 5E), whereas it was negatively correlated with the proportion of $Ly6C^+$ low monocytes (Fig. 5F). By contrast, no significant correlations were observed with the proportions of other immune cell subsets (Fig. 5A–D). Moreover, the latency to enter the open arms was positively correlated with the S100A10 levels in $CD45^+$ immune cells (Fig. 5G), $CD8^+$ T cells (Fig. 5I), and total monocytes (Fig. 5J), with no significant associations noted for the S100A10 levels in other immune populations (Fig. 5H,K,L). Taken together, these data demonstrate that alterations in the proportions of peripheral immune cells and increased S100A10 levels in $CD8^+$ T cells and monocytes are closely associated with CSD-induced anxiety-like behaviors in mice. These immune parameters and peripheral p11 levels may therefore serve as valuable biomarkers of anxiety-related behavioral abnormalities after CSD.

3.4 Effects of CSD on Serum Proinflammatory Cytokines, BBB, and Hippocampal Microglial Activation

To further evaluate the effects of CSD on BBB integrity, hippocampal ZO-1 expression was examined through immunofluorescence staining. Compared with the control group, the ZO-1 MFI in the DG subregion was significantly decreased in the CSD group, whereas that in the CA1 and CA3 subregions exhibited nonsignificant decreasing trends (Fig. 6A,B). Next, immunofluorescence staining was performed to examine Iba1 (a microglial marker) expression in the hippocampus. The results revealed that the number of Iba1-positive cells in the CA1, CA3, and DG subregions was significantly increased in the CSD group compared with the control group (Fig. 6C,D). Collectively, these results indicate that CSD disrupts the BBB and induces microglial activation in the hippocampus.

To determine the effects of CSD on inflammatory responses, the serum protein levels of the proinflammatory cytokines IL-6, IL-1β, and TNF-α were analyzed through ELISA. IL-6, IL-1β, and TNF-α levels significantly increased in the CSD group (**Supplementary Fig. 2A–C**). qPCR results unveiled that, compared with the control group, *Il6* and *Tnf* mRNA expressions in the hippocampus significantly increased in the CSD group, whereas *Il1b* mRNA expression exhibited a nonsignificant increasing trend (**Supplementary Fig. 2D–F**). We further examined microglial polarization in the hippocampus through qPCR. The *Cd86* mRNA expression significantly decreased, whereas the *Arg1* mRNA expression significantly increased in the CSD group, with no significant differences observed in *Nos2* and *Mrc1* (**Supplementary Fig. 2G,H**). Collectively, these findings suggest that CSD elevates proinflammatory cytokine levels in peripheral blood and drives microglial activation in the hippocampus.

3.5 CSD Changes the Hippocampal Metabolome in Mice

Given the key role of the hippocampus in emotional regulation and the close association between metabolic homeostasis and anxiety-like behaviors, untargeted metabolomics was performed to systematically deter-

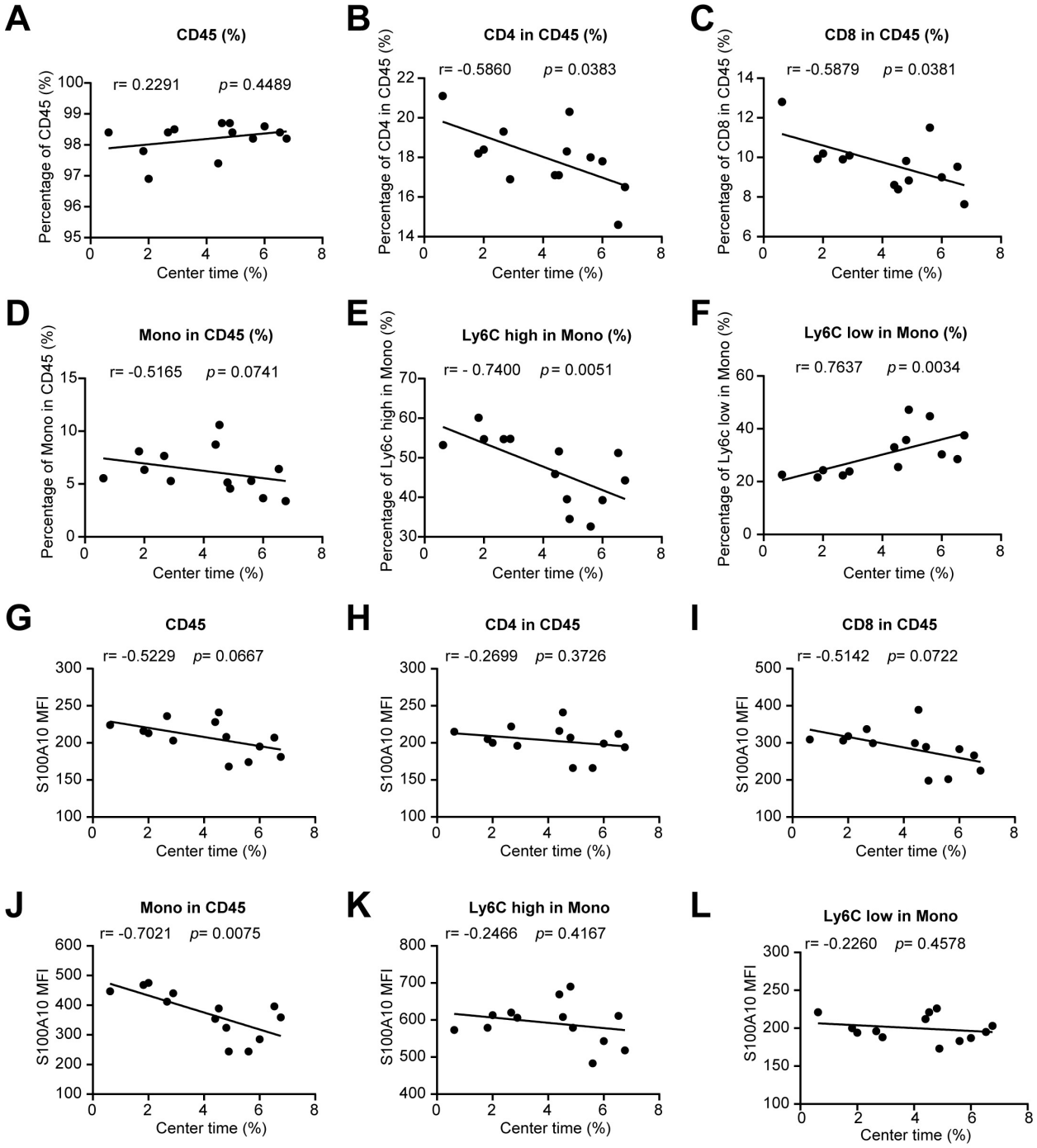


Fig. 4. Correlation analysis between the core parameter of the OFT and peripheral blood T cells, monocytes, and S100A10 levels. (A–F) Correlation analyses between the proportion of time spent in the central zone of OFT and the percentages of peripheral blood immune cells, including $CD45^+$ cells (A), $CD4^+$ T cells (B), $CD8^+$ T cells (C), monocytes (D), $Ly6C^+$ high monocytes (E), and $Ly6C^+$ low monocytes (F). (G–L) Correlation analyses between the proportion of time spent in the central zone of OFT and S100A10 levels in peripheral blood cell subsets, including $CD45^+$ cells (G), $CD4^+$ T cells (H), $CD8^+$ T cells (I), total monocytes (J), $Ly6C^+$ high monocytes (K), and $Ly6C^+$ low monocytes (L). Spearman correlation analysis was applied to (A–F), and Pearson correlation analysis was applied to (G–L). The correlation coefficient (r value) and statistical significance (*p* value) are labeled in each figure.

mine the effects of CSD on hippocampal metabolic characteristics in mice (Figs. 7,8). We explored the potential relationship between central metabolic changes and anxiety-like behaviors.

In total, 402 annotated metabolites at identification confidence Level 1, including lipids, amino acid derivatives, and nucleotides, were identified in the hippocampus. (Fig. 7A,B). In total, 157 differential metabolites were

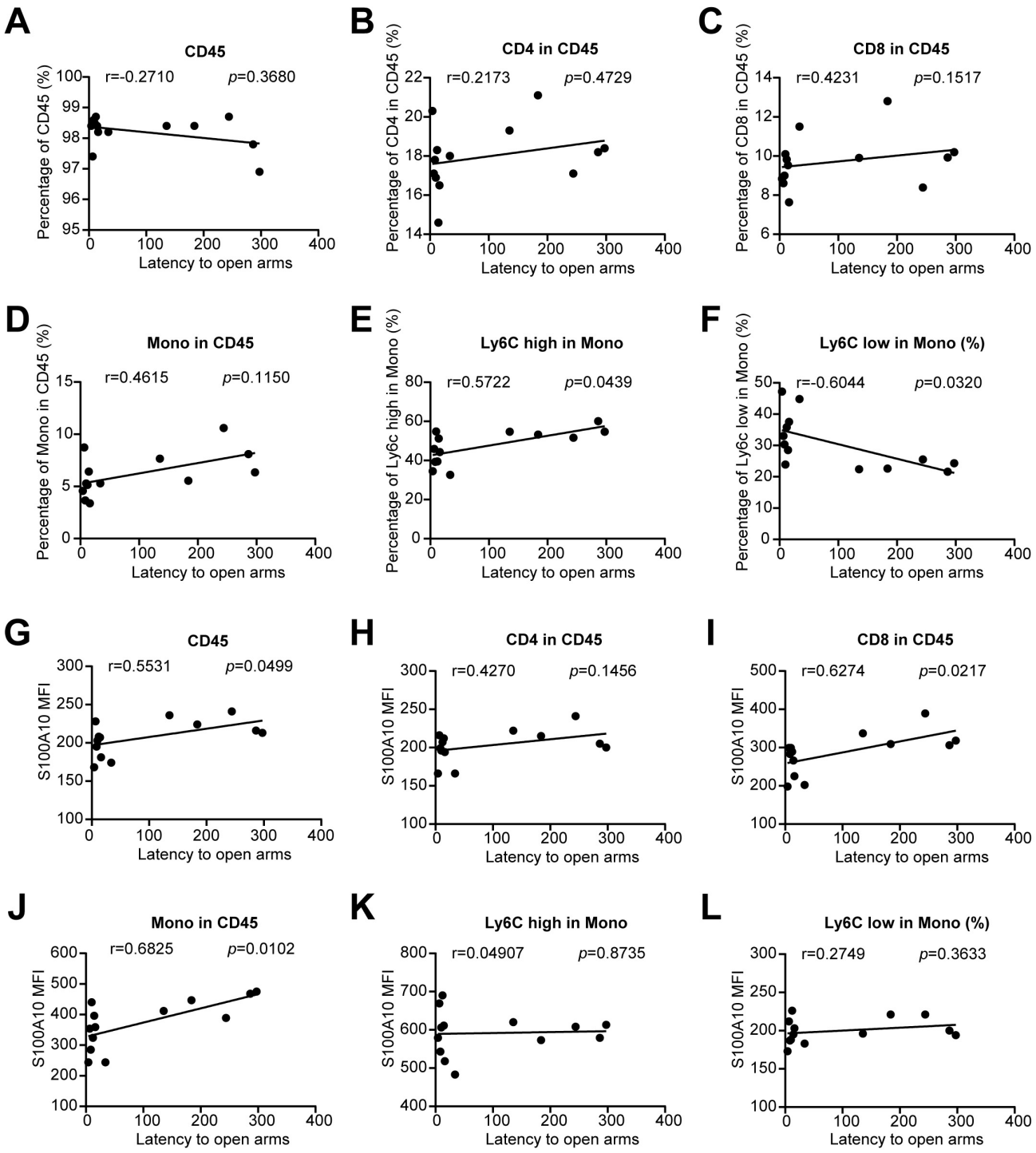


Fig. 5. Correlational analysis between the core parameter of the EPM test and peripheral blood T cells, monocytes, and S100A10 levels in mice. (A–F) Correlation analyses between the latency to open arms in the EPM test and the percentages of peripheral blood immune cells, including $CD45^+$ cells (A), $CD4^+$ T cells (B), $CD8^+$ T cells (C), monocytes (D), $Ly6C^+$ high monocytes (E), and $Ly6C^+$ low monocytes (F). (G–L) Correlation analyses between the latency to open arms in the EPM test and S100A10 levels in the peripheral blood cell subsets, including $CD45^+$ cells (G), $CD4^+$ T cells (H), $CD8^+$ T cells (I), total monocytes (J), $Ly6C^+$ high monocytes (K), and $Ly6C^+$ low monocytes (L). Control group, n = 7; CSD group, n = 6. Spearman correlation analysis was applied to (A–F), and Pearson correlation analysis was applied to (G–L). The correlation coefficient (r value) and statistical significance (*p* value) are labeled in each figure.

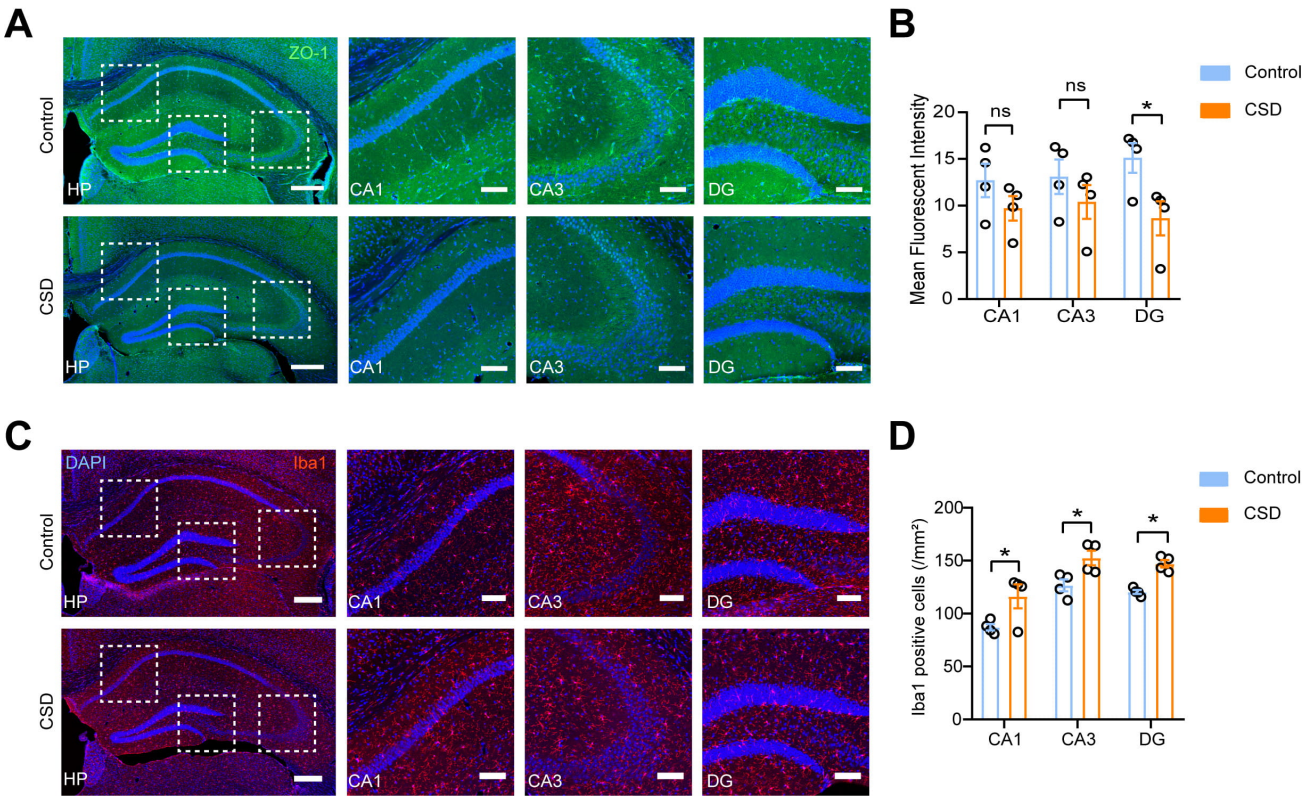


Fig. 6. Effects of CSD on blood–brain barrier integrity and neuroinflammation in the hippocampus region. (A,B) Representative immunofluorescence images showing the ZO-1 expression in the CA1, CA3, and DG subregions of the hippocampus (A), and the quantitative analysis of mean fluorescence intensity (B) in the control and CSD mice. Scale bar = 300 μm (left panel); scale bar = 100 μm for magnified images (right panels). (C,D) Representative immunofluorescence staining for Iba-1 in hippocampal CA1, CA3, and DG subregions (C), and the quantification of Iba-1-positive cells (D). Scale bar = 300 μm (left panel); scale bar = 100 μm for magnified images (right panels). Control group, n = 4; CSD group, n = 4. Data are presented as the mean ± S.E.M.. and analyzed using an unpaired two-tailed Student's *t*-test. **p* < 0.05; ns, no significance.

identified based on the screening criteria. Compared with the control group, 62 metabolites were upregulated, and 95 were downregulated in the CSD group (Fig. 7C). The overall distribution of these differential metabolites is shown in the volcano plot (Fig. 7D).

To determine the central metabolic regulatory mechanism underlying anxiety-like behaviors, nine of the identified differential metabolites were analyzed (Fig. 8). Compared with the control group, ginsenoyne K, glutathione trisulfide, garcinia biflavonoid 2, and casimiroin were significantly upregulated in the CSD group. By contrast, acorusnol, sarcosterol, N-(1,1-dimethyl-2-hydroxyethyl) arachidonoyl amine, PI (20:4/0:0), and 2-hydroxyclomipramine were significantly downregulated in the CSD group (Fig. 8A–I).

To further investigate the interactions among these metabolites, we performed correlation analysis. The result revealed that these nine differential metabolites formed a complex interaction network (Fig. 8J). Overall, four upregulated metabolites including ginsenoyne K, glutathione trisulfide, garcinia biflavonoid 2, and casimiroin were negatively correlated with acorusnol, sarcosterol, N-(1,1-dimethyl-2-hydroxyethyl) arachidonoyl amine, PI (20:4/0:0), and 2-hydroxyclomipramine. Altogether, these findings suggest that CSD disrupts the metabolites in the hippocampus, possibly linking to anxiety-like behaviors.

3.6 Correlation Between Hippocampal Metabolites and Anxiety-Like Behaviors

To elucidate the relationship between hippocampal metabolites and anxiety-like behaviors, correlation analysis was performed between the percentage of time spent in the central zone in the OFT and the aforementioned key differential hippocampal metabolites. The levels of hippocampal ginsenoyne K, glutathione trisulfide, garcinia biflavonoid 2, and casimiroin were negatively correlated with the time spent in the central zone (Fig. 9A–D). The levels of downregulated metabolites, including acorusnol and phosphatidylinositol PI [PI (20:4/0:0)], were positively correlated with the time spent in the central zone, whereas no significant correlations were observed for sarcosterol, N-(1,1-dimethyl-2-hydroxy-ethyl) arachidonoyl amine, and 2-hydroxyclomipramine (Fig. 9E–I).

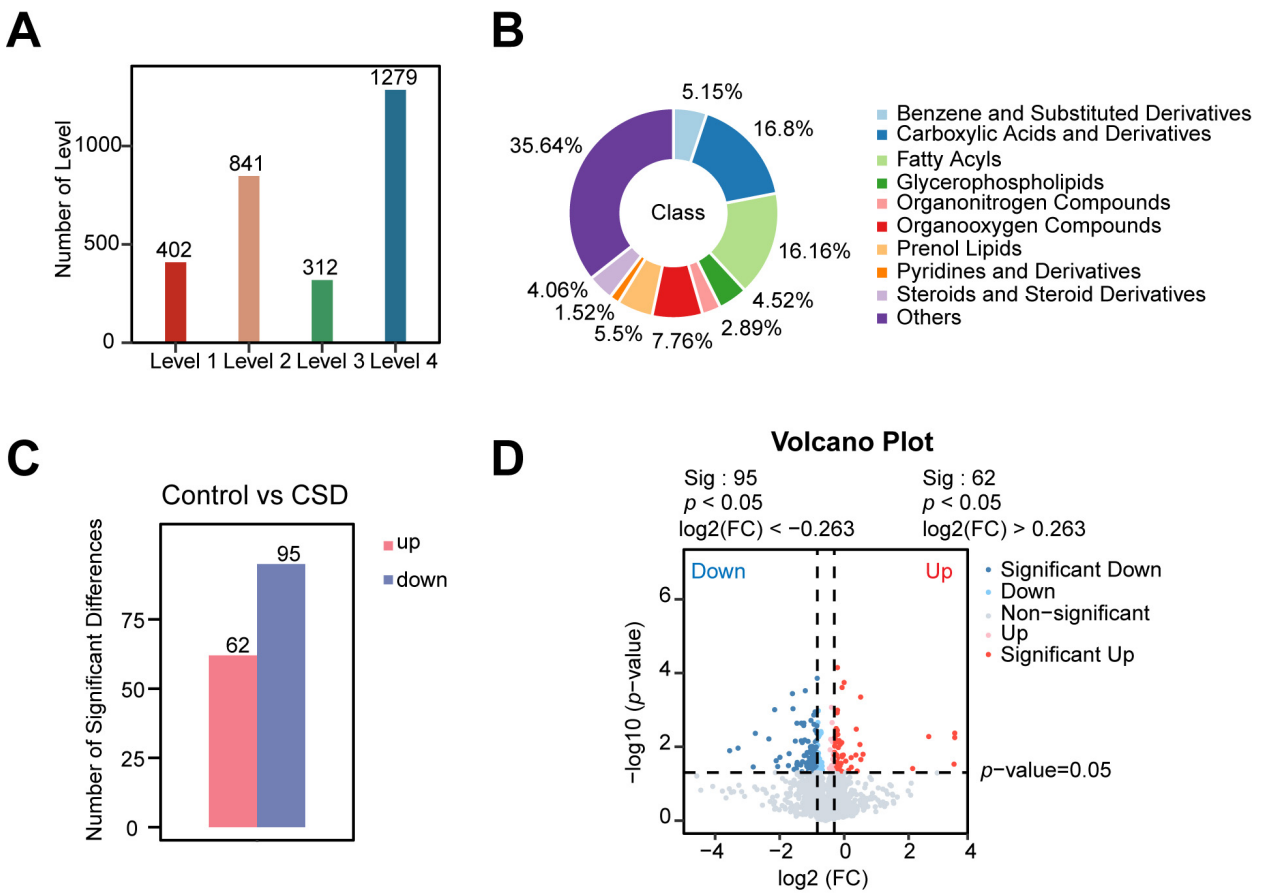


Fig. 7. Untargeted metabolomics analysis of the hippocampal region after CSD. (A) Bar plot depicting the number of metabolites at four levels. A total of 402, 841, 312 and 1279 annotated metabolites were classified into Level 1, Level 2, Level 3 and Level 4, respectively. (B) Pie chart showing the proportion of metabolites by chemical class in the hippocampal region. (C) Bar graph displaying the number of significantly upregulated and downregulated differential metabolites in CSD mice relative to the control. (D) Volcano plot visualizing all differential metabolites. Red dots represent significantly upregulated metabolites, blue dots represent significantly downregulated metabolites, and gray dots indicate metabolites with no statistically significant expression changes.

To further identify the key biological pathways associated with CSD-induced changes in hippocampal metabolites, KEGG pathway enrichment analysis was conducted. The enriched pathways could be broadly classified into three categories (Fig. 10). The first comprised pathways involved in cellular signaling and intracellular communication, including the cyclic adenosine monophosphate (cAMP) signaling pathway, gap junctions, and efferocytosis. The second included core metabolic pathways, such as cysteine and methionine metabolism; glutathione metabolism; alanine, aspartate, and glutamate metabolism; and glycerophospholipid metabolism. The third category consisted of other related pathways, such as hormone signaling and renin secretion. Additionally, these pathways are closely associated with the maintenance of central emotional homeostasis. Collectively, these findings suggest that CSD-induced alterations in these metabolites are correlated with the emergence of anxiety-like behaviors.

4. Discussion

This study systematically investigated the mechanisms underlying CSD-induced anxiety-like behaviors in mice, with a particular focus on peripheral immune alterations, central neuroinflammation, and hippocampal metabolic remodeling. Our findings demonstrate that 7 days of CSD induced robust anxiety-like behaviors, accompanied by disrupted peripheral monocyte homeostasis, increased S100A10 levels in specific immune cell populations, and profound metabolic remodeling in the hippocampus. Notably, all these peripheral and central molecular alterations were significantly correlated with anxiety-like behavioral indices. Moreover, CSD elevated circulating levels of proinflammatory cytokines, disrupted hippocampal BBB integrity, and promoted hippocampal neuroinflammation. Collectively, these data indicate that CSD-driven anxiety-like behaviors are closely associated with peripheral immune dysregulation, hippocampal neuroinflammation, and metabolic imbalance.

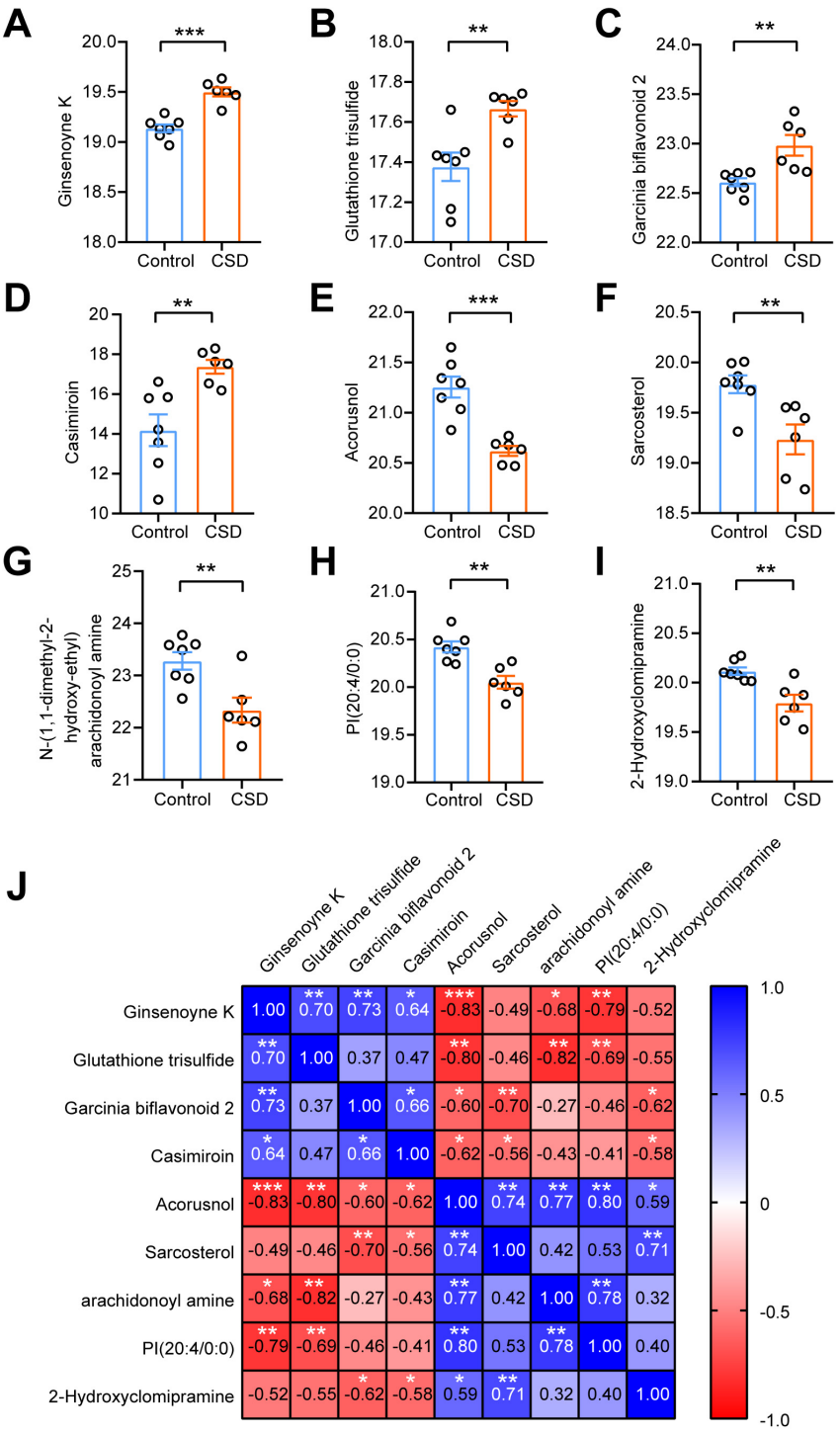


Fig. 8. Relative abundance of representative differential metabolites in the hippocampal region and their correlational analyses. (A–I) Bar graphs displaying the relative levels of nine key altered metabolites between the two groups: (A) Ginsenoyne K; (B) Glutathione trisulfide; (C) Garcinia biflavonoid 2; (D) Casimiroin; (E) Acorusnol; (F) Sarcosterol; (G) N-(1,1-dimethyl-2-hydroxy-ethyl) arachidonoyl amine; (H) PI(20:4/0:0); (I) 2-Hydroxyclomipramine. Control group, n = 7; CSD group, n = 6. Data are presented as the mean ± S.E.M.. Two-tailed unpaired *t*-test. $^{**}p < 0.01$ and $^{***}p < 0.001$. (J) Correlation heatmap illustrating pairwise correlation coefficients among the nine differential metabolites. Correlation analyses were performed using Pearson's test. $^{*}p < 0.05$, $^{**}p < 0.01$ and $^{***}p < 0.001$. Blue color denotes positive correlation, whereas red color represents negative correlation. Asterisks indicate the statistical significance of correlation coefficients.

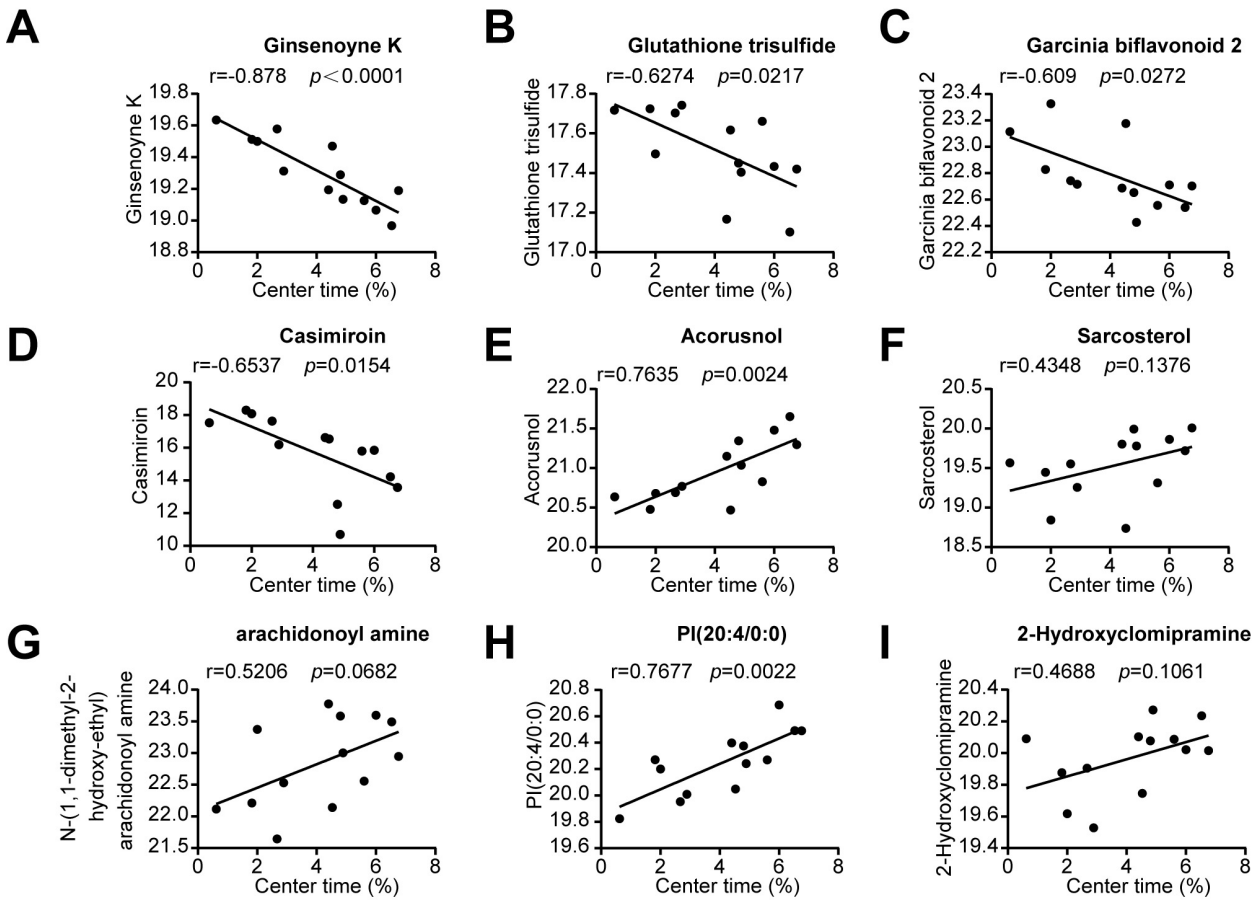


Fig. 9. Correlation analysis between core anxiety-like behavior parameters and the relative abundance of key differential metabolites. (A–I) Scatter plots with linear regression lines demonstrating the correlation between time spent in the central zone (%) and the levels of nine characteristic differential metabolites: (A) Ginsenoyne K; (B) Glutathione trisulfide; (C) Garcinia biflavonoid 2; (D) Casimiroin; (E) Acorusnol; (F) Sarcosterol; (G) N-(1,1-dimethyl-2-hydroxy-ethyl) arachidonoyl amine; (H) PI(20:4/0:0); (I) 2-Hydroxyclomipramine. Control group, n = 7; CSD group, n = 6. All correlation analyses were performed using Pearson's test, with the correlation coefficient (r value) and statistical significance (*p* value) labeled in each subfigure.

In the present study, a CSD model was established to evaluate the effects of CSD on anxiety-like behaviors. Behavioral assessments confirmed that CSD induced a typical anxiety-like phenotype. Although the total locomotor distance in the OFT was slightly reduced, the core anxiety-related indices were significantly altered. The slight reduction in total locomotor activity is therefore more likely to represent a concurrent progression of the anxiety-like condition rather than an independent confounding factor. Reduced exploratory motivation is a characteristic feature of anxiety disorders. CSD may increase the fear of the unknown and reduce the willingness to explore, resulting in decreased locomotor activity [33,34], without affecting the specificity of the anxiety behavior.

Neuroimmune crosstalk has emerged as a central mechanism in neuroimmunology that drives the onset and progression of mood disorders [14]. Accumulating evidence highlights the key role of inflammatory cytokines in the pathogenesis of psychiatric disorders, including post-traumatic stress disorder (PTSD) and MDD [35]. A clinical study has demonstrated markedly elevated circulating proinflammatory cytokines in patients with anxiety disorders [36]. Consistently, preclinical animal studies reveal robust microglial activation and concurrent upregulation of proinflammatory cytokines in the brain of anxiety-like phenotype mice [37]. Furthermore, central neuroinflammation can precipitate a broad spectrum of neuropsychiatric disorders, with both humoral and cellular immune responses contributing to disease progression [38]. Consistent with these previous findings, we systematically evaluated peripheral proinflammatory cytokine levels, hippocampal expression of the tight junction protein ZO-1, and microglial activation in mice following CSD. Our results demonstrated that CSD markedly elicited pronounced anxiety-like behaviors, elevated peripheral and hippocampal proinflammatory cytokine levels, compromised BBB integrity, and promoted microglial activation. These findings align well with previously published findings.

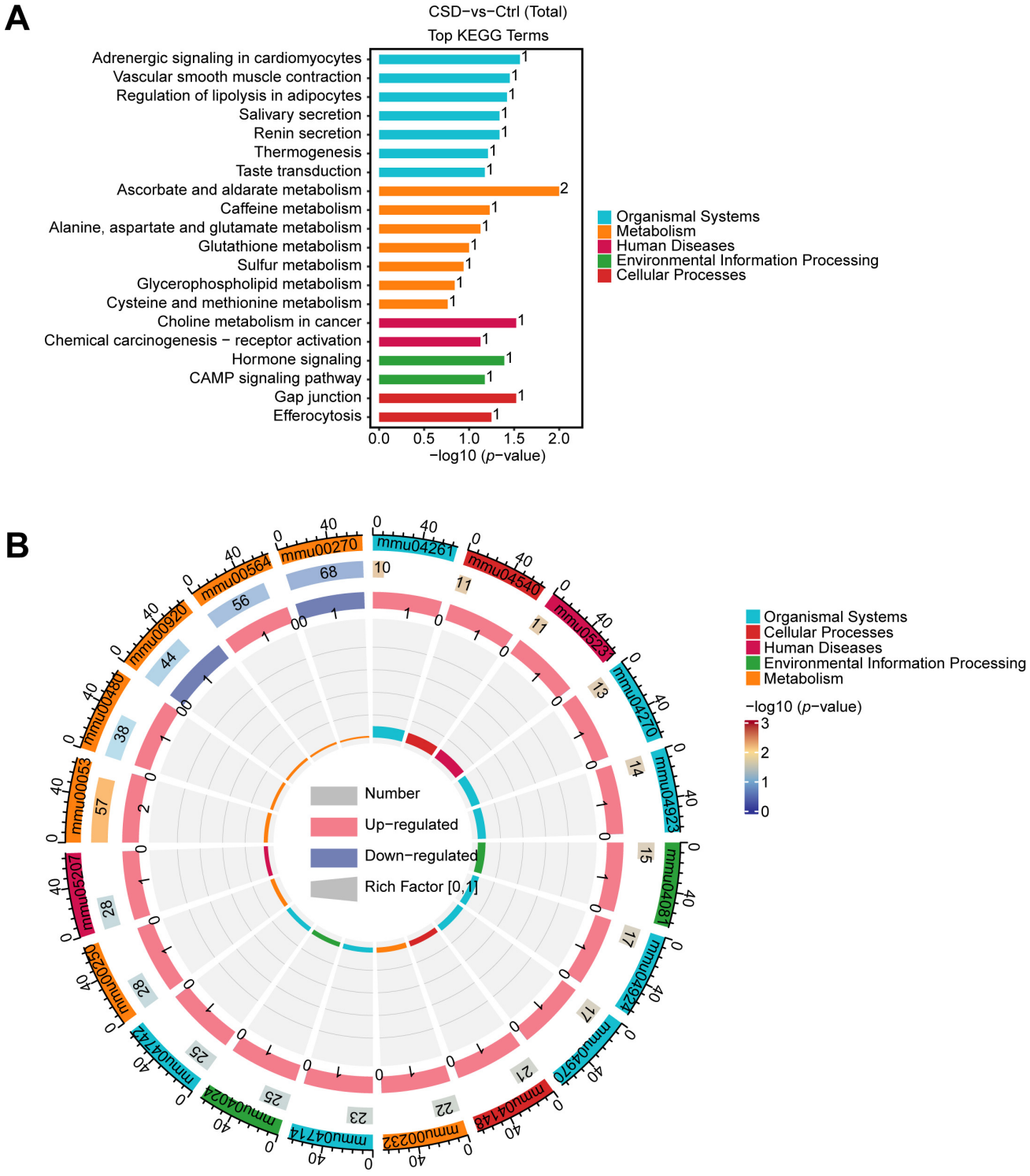


Fig. 10. KEGG Analysis of Metabolites in the Hippocampal Region after CSD. (A) Bar chart displaying the top enriched KEGG pathways ranked by –log10 (*p*-value). The pathways are color-coded according to five major KEGG functional categories: Organismal Systems, Metabolism, Human Diseases, Environmental Information Processing, and Cellular Processes. The x-axis represents the –log10 transformed *p*-value of enrichment. (B) Circular plot of KEGG enrichment analysis.

In the present study, we focused on two key immune indices: monocyte subset distribution and S100A10 levels. Although CSD did not significantly alter the proportions of total T cells or total monocytes, it considerably shifted monocyte subset composition by increasing the proportion of proinflammatory Ly6C^{+} high monocytes while decreasing the proportion of anti-inflammatory Ly6C^{+} low monocytes. A study has demonstrated that Ly6C^{+} high mono-

cytes promote neuroinflammation by releasing proinflammatory cytokines in the brain [39]. However, the reduced anti-inflammatory and tissue repair functions of the $Ly6C^+$ low subset can further aggravate immune imbalance and central inflammatory responses. This phenomenon is consistent with the functional characteristics of $Ly6C^+$ monocyte subsets. As classical monocytes, $Ly6C^+$ high monocytes depend on C-C motif chemokine receptor 2 (CCR2) signaling for migration and inflammatory amplification, whereas $Ly6C^+$ low nonclassical monocytes contribute to vascular homeostasis and anti-inflammatory repair through CX3C motif chemokine receptor 1 (CX3CR1) [40]. The chronic stress-induced imbalance in monocyte subsets observed in this study is consistent with previous findings suggesting that remodeling of monocyte subset distribution contributes to the amplification of local inflammation [41,42]. These findings further suggest that monocyte subset imbalance and central neuroinflammation may contribute to CSD-induced anxiety-like behaviors.

S100A10 is a multifunctional calcium-binding protein with pivotal roles in the pathogenesis of inflammatory diseases and mood disorders. S100A10-knockout mice exhibit increased susceptibility to endotoxin-induced shock [43]. S100A10 loss augments the proinflammatory activity of neutrophils and elevates the secretion of proinflammatory cytokines, thereby exacerbating intestinal inflammation [44]. In rodent studies, S100A10 colocalized with diverse protein molecules and modulated multiple neurotransmitter systems, including γ-aminobutyric acid, acetylcholine, glutamate, and monoamine neurotransmitters [45]. In transgenic fluorescent reporter mice, S100A10 was expressed across multiple brain regions, including the cerebral cortex, nucleus accumbens (NAc), hippocampus, amygdala, hypothalamus, and raphe nuclei—many of these regions are closely associated with emotional processing and reward circuitry [45,46]. S100A10-knockout mice exhibit depressive-like behavior [21]. Notably, S100A10 exerts divergent regulatory effects on mood dysfunction in distinct brain subregions. S100A10 is highly enriched in the medial prefrontal cortex (mPFC) and NAc; its deletion disrupts local field potential coupling between these two regions, drives hyperactivity of mPFC neurons, and ultimately induces anxiety and impaired emotional recognition [47]. Conversely, hippocampal p11 knockdown abolishes the sustained antidepressant efficacy of ketamine [48]. Intriguingly, overexpression of p11 in lateral habenula mediates depression-like behavior [49]. Mounting evidence further links S100A10-dependent regulation of mood disorders to neurotransmitter dyshomeostasis. In mice, p11 co-localizes with cholinergic interneurons in the NAc, where it modulates acetylcholine (ACh) release to facilitate dopamine efflux and participate in the regulation of depressive-like symptomatology [50]. Under anxious states, p11 deficiency curtails ACh release in the ventral tegmental area (VTA) and disrupts dopamine (DA) signaling within the NAc, further exacerbating dysfunctional emotional circuitry [25]. Accordingly, the present study did not characterize the association between CSD-induced anxiety-like behaviors and S100A10 levels in key brain regions including the mPFC, NAc and VTA. We also did not quantify dynamic shifts of acetylcholine, dopamine and other key neurotransmitters within these areas. Therefore, S100A10 expression in the brain, neurotransmitter release, and their exact downstream molecular mechanisms remain to be systematically explored in future work.

The present study primarily investigated the potential of peripheral immune cells and their S100A10 expression as circulating biomarkers for anxiety-like behavioral abnormalities. However, the regulatory role of altered S100A10 expression on peripheral immune cells is fundamentally distinct from that of brain-resident S100A10 in mediating depressive- and anxiety-related behaviors. Additionally, the deficiency of S100A10 increases the proinflammatory activity of neutrophils, promotes the release of proinflammatory cytokines, and exacerbates intestinal inflammation [44]. Clinical studies have reported that S100A10 levels in the peripheral blood T cells and adrenocorticotropic hormone are significantly higher in patients with major depressive disorder than in healthy controls (HCs) [22]. Furthermore, S100A10 levels in monocytes are increased in patients with Parkinson's disease (PD) comorbid with depression. Additionally, S100A10 levels in $CD8^+$ cells of patients with PD (regardless of the presence of comorbid depression) are significantly higher than those in HCs [25]. The results of the present study suggest that CSD regulates S100A10 in a cell-specific manner. We found that S100A10 levels in $CD45^+$ leukocytes, $CD8^+$ T cells, and total monocytes were significantly upregulated, consistent with previous findings [22,25].

As a central brain region involved in emotional regulation, the hippocampus plays a critical role in maintaining metabolic homeostasis and supporting emotional regulation [51,52]. Previous studies have shown that chronic physical stress primarily disrupts hippocampal lipid and glutamate metabolism, characterized by reduced glutamate levels and impaired lipid homeostasis. Notably, the chronic unpredictable mild stress model is also established by the activation of inflammatory pathways, triggering anxiety-like behaviors. However, psychological stress affects cell signaling and neurodevelopment-related metabolic pathways, disrupting hippocampal neurogenesis and synaptic plasticity [53]. In the present study, untargeted metabolomics was performed to systematically investigate the regulatory effects of CSD on the mouse hippocampal metabolic profile. We aimed to clarify the functional characteristics of differential metabolites and their intrinsic association with anxiety-like behaviors. In total, 157 differential hippocampal metabolites were identified. KEGG pathway enrichment analysis revealed significant enrichment in the cAMP signaling pathway, glutathione metabolism,

glycerophospholipid metabolism and other pathways. Additionally, the enriched cAMP-signaling pathway plays a key role in synaptic plasticity and emotional regulation; the glutathione metabolism pathway is essential for regulating oxidative stress; and glycerophospholipid metabolism contributes to the maintenance of cell membrane function. Dysfunction of these pathways further confirms that CSD affects hippocampal function via multidimensional metabolic interference. Notably, fold change (FC) $\geq$1.2 combined with nominal $p < 0.05$ was adopted as the screening criterion for differential metabolites in this study, consistent with the criterion used in a prior non-targeted metabolomics study of hippocampal tissue [54]. This relatively lenient threshold was chosen to expand the scope of metabolite screening and retain subtle metabolic perturbations with potential biological implications. Importantly, this approach did not include multiple testing correction; therefore, these metabolites are preliminary candidates and require further validation. However, a lenient threshold may increase the risk of false-positive metabolite identification. Furthermore, the present study only preliminarily identified correlations between metabolites and anxiety-like behaviors. Targeted functional experiments are still required to verify whether these metabolites are necessary and sufficient to regulate anxiety-like behaviors before they can be regarded as candidate targets for subsequent mechanism exploration and therapeutic intervention.

In the present study, the upregulated metabolites in the CSD group were negatively correlated with the percentage of time spent in the central zone of OFT. In contrast, downregulated metabolites under CSD were positively correlated with these anxiety-related indicators. Among these metabolites, ginsenoyne K and PI (20:4/0:0) showed the strongest correlations with anxiety-related behavior. A study has shown that multiple constituents of Panax ginseng modulate emotion-related behaviors [55], implying a potential role for ginsenoyne K in these processes. Furthermore, ginsenoyne analogs have been shown to promote microglial polarization toward an anti-inflammatory M2 phenotype, suppress activation of the nucleotide-binding domain and leucine-rich repeat-containing protein family pyrin domain-containing 3 (NLRP3) inflammasome and the NF-κB-signaling pathway to reduce central neuroinflammation, and preserve synaptic plasticity through antioxidative mechanisms and regulation of brain-derived neurotrophic factor (BDNF) expression [56]. An existing review has demonstrated that at the early stage of stress, organisms activate compensatory protective mechanisms by upregulating metabolites. However, insufficient compensatory capacity fails to counteract tissue damage, leading to sustained accumulation of neuroinflammation and persistent anxiety-like behaviors [57]. Additional research corroborates that sleep deprivation acutely upregulates endogenous metabolites as an adaptive buffer against oxidative stress, yet persistent sleep deprivation progressively depletes these intrinsic protective reservoirs [58]. Collectively, the findings from the above literature offer a contextual basis for the elevation of ginsenoyne K observed in this study.

Given the central role of microglia-mediated neuroinflammation in emotional regulation, we simultaneously measured neuroinflammatory markers in the mouse hippocampus. Our results revealed that CSD induced microglial activation and upregulated the pro-inflammatory cytokines *Il6* and *Tnf*, alongside increased expression of the M2 polarization-associated gene *Arg1*. In line with this, recent evidence suggests that chronic stress exacerbates hippocampal neuroinflammation and microglial activation, contributing to depression-like behaviors [59]. It is important to acknowledge that the qPCR detection of this M2 marker was conducted on a limited number of animals, which requires careful interpretation of the results. Meanwhile, *Il1b* only displayed a modest rising trend without statistical significance. We attribute this inconsistent expression pattern to the restricted sample. A larger sample size is required to obtain consistent expression changes of pro-inflammatory cytokines. Beyond this observation, the elevation of microglial activation alongside increased expression of the M2 polarization-associated gene *Arg1* in the hippocampus needs further in-depth investigation. As reviewed previously, microglial activation cannot be simply classified into an oversimplified M1/M2 polarization. Under different stimuli, microglia can express both pro- and anti-inflammatory polarized phenotypes [60]. Under physiological homeostasis, resident central microglia exhibit a resting M2-like phenotype. In animal models of autoimmune central demyelinating diseases, lesions are dominated by pro-inflammatory M1 macrophages in the acute phase. At the disease peak and repair stage, the proportion of M2-type cells in lesions rises greatly [61]. Previous research verifies that CSD triggers peripheral inflammation and activates hippocampal microglia. In this model, *Il1b* only shows an upregulated trend without statistical significance, alongside higher expression of M2 polarization markers such as *Arg1* [62]. Other research has shown that chronic sleep fragmentation triggers microglia-driven neuroinflammation, accompanied by upregulation of markers of both M1 and M2 polarization [63]. Overall, these prior studies offer a reasonable explanation for our finding of elevated pro-inflammatory cytokines alongside enhanced M2 polarization. These findings imply that analyses of microglial polarization and pro-inflammatory cytokines should be supported by sufficient animal samples to improve the interpretability of the relevant outcomes.

PI is a key component of cell membrane phospholipids and provides an essential structural foundation for neural signal transmission [64,65]. Furthermore, phosphatidylinositol-3-phosphate [PI(3)P], a specific phosphorylated derivative of PI, plays an important role in regulating synaptic plasticity [66]. In the hippocampus, PI4P

synthesis is mainly involved in the regulation of synaptic plasticity [67]. Previous studies have shown that PI4P levels on the dendritic plasma membrane of hippocampal neurons dynamically change in response to synaptic activity, thereby modulating the structural maturation and functional plasticity of dendritic spines via α-amino-3-hydroxy-5-methyl-4-isoxazolepropionic acid (AMPA) receptors [67]. This mechanism is highly consistent with the findings of the present study, which showed CSD-induced downregulation of PI. Chronic social defeat stress can significantly downregulate PI4KIIIβ expression and phosphoinositide levels in the VTA, leading to dysfunction of dopaminergic neurons and establishing a direct association between PI metabolic imbalance and synaptic impairment in emotion-related brain regions [68]. As a chronic stressor, CSD may similarly disrupt the balance of this regulatory network, triggering parallel abnormalities across multiple PI subtypes, brain regions, and signaling pathways. Such disturbances can disrupt synaptic functions and the homeostasis of emotional circuits, ultimately contributing to the development of anxiety-like behaviors. These findings further elaborate on the understanding of PI metabolism in stress-related emotional disorders and suggest that the PI metabolic pathway may represent a promising molecular target for developing anxiety intervention strategies.

Limitations

We systematically integrated peripheral monocyte subset distribution, S100A10 expression profiles, hippocampal metabolomics, neuroinflammatory markers, and behavioral indices to construct a multidimensional correlative network underlying CSD-triggered anxiety-like phenotypes. Nevertheless, the present study has several limitations that should be acknowledged. Sleep homeostasis is essential for maintaining systemic immune homeostasis and central metabolic balance. Our findings demonstrate that CSD promotes persistent mobilization of bone marrow-derived monocytes, disrupts the balance of peripheral Ly6C monocyte subsets, impairs BBB integrity, and further induces excessive hippocampal microglial activation and local accumulation of proinflammatory cytokines. Nevertheless, the optimal time window for sleep homeostasis restoration, as well as whether sleep recovery can reverse CSD-induced behavioral abnormalities and the associated peripheral and central molecular alterations, remain to be determined. The present study did not perform *in vivo* functional validation via monocyte-specific conditional S100A10 knockout mice. Future studies will employ monocyte-targeted Cre-inducible transgenic reporter lines to selectively ablate S100A10 in monocytes, which will further delineate the indispensable function of this gene in driving anxiety-like behavioral phenotypes. Furthermore, CSD facilitates the infiltration of peripheral immune cells into the central nervous system, which subsequently participates in neuroinflammation and the regulation of emotional behaviors. This study characterizes microglial activation and phenotypic transformation without comprehensive localization analysis of infiltrating immune cells in the brain. Follow-up research will further dissect the activation and infiltration of central immune cells under anxiety-like conditions to complement the mechanistic framework underlying central immune regulation. Moreover, validation in clinical cohorts is required to determine whether peripheral monocyte subset distribution and peripheral p11 levels could serve as candidate clinical biomarkers for sleep disturbance-related anxiety.

In summary, the present study demonstrates that CSD provokes anxiety-like phenotypes through coordinated crosstalk between the immune system and central metabolism. These findings may support the development of targeted intervention strategies and facilitate the discovery of potential biomarkers for sleep disturbance-related emotional disorders.

5. Conclusion

The present study aimed to characterize biological alterations associated with CSD-related anxiety-like behaviors and to investigate the parallel association between peripheral immunity and central metabolism. Alongside CSD-related anxiety-like phenotypes, peripheral monocyte proportions were altered, with elevated proinflammatory $Ly6C^+$ high monocytes. Consequently, CSD specifically upregulates S100A10 expression on $CD45^+$ cells, $CD8^+$ T cells, and total monocytes, which indicates a significant association with anxiety-like behaviors. CSD disrupted the BBB, promoted microglial activation, and elevated the levels of proinflammatory cytokines in the peripheral blood and hippocampal tissue. Hippocampal metabolomic profiling unveiled that CSD can reshape its metabolic landscape. Our findings may provide promising leads for interventions targeting sleep disturbance-related emotional disorders and facilitate the identification of candidate biomarkers for such disorders.

Availability of Data and Materials

The data are available from the corresponding authors upon reasonable request.

Author Contributions

RH, HW, XS, and ZL designed the research study. XS, ZH, and ZL performed the main experiments of this study. YL, PF and QH participated in animal experiments and flow cytometry data detection and analysis. YL and HW provided experimental guidance for this project. RH, ZH, and XS wrote the initial draft. All authors contributed to editorial changes in the manuscript. All authors revised and approved the final manuscript. All authors have participated sufficiently in the work and agreed to be accountable for all aspects of the work.

Ethics Approval and Consent to Participate

All animal experiments were approved by the Institutional Animal Care and Use Committee of Xinxiang Medical University (IACUC Protocol No. HYYLL-2025790), and we complied with all relevant ethical regulations. Every effort was made to minimize the number of animals used and reduce their suffering throughout the study. The study did not involve human participants, so no informed consent was required. All protocols were designed to adhere to the 3Rs principles of animal research and were periodically reviewed by the IACUC to ensure ongoing compliance with ethical standards. The study was carried out in accordance with the ARRIVE guidelines.

Acknowledgment

We sincerely thank Dr. Zhitao Gao (Xinxiang Medical University) for their technical guidance and constructive comments. Additionally, we thank other laboratory members (excluding this manuscript's authors) for their support in animal care and sample preparation.

Funding

This work was financially supported by the National Natural Science Foundation of China (Grant No. 32000708 and U21A20366), and Key Scientific Research Projects of Higher Education Institutions in Henan Province (Grant No. 24A320008), and China National University Student Innovation & Entrepreneurship Development Program of Xinxiang Medical University (Grant No. 202410472007), and the Natural Science Foundation of Henan Province (Grant No. 252300423082), and Higher Education Discipline Innovation Project (111 Project, No. D20036).

Conflicts of Interest

The authors declare no conflicts of interest.

Supplementary Material

Supplementary material associated with this article can be found, in the online version, at https://doi.org/10.31083/JIN52481.

References

[1] Penninx BW, Pine DS, Holmes EA, Reif A. Anxiety disorders. Lancet (London, England). 2021; 397: 914–927. https://doi.org/10.1016/S0140-6736(21)00359-7

[2] Szuhany KL, Simon NM. Anxiety Disorders: A Review. JAMA. 2022; 328: 2431–2445. https://doi.org/10.1001/jama.2022.22744

[3] Zhou J, Li S, Song Y, Ying J, Luo Z, Shan S, et al. Global, regional, and national trends in the burden of anxiety disorders from 1992 to 2021: an age–period–cohort analysis based on the Global Burden of Disease Study 2021. Depression and Anxiety. 2025; 2025: 4178541. https://doi.org/10.1155/da/4178541

[4] Uher R. The global impact of anxiety disorders. The Lancet. Psychiatry. 2023; 10: 239–240. https://doi.org/10.1016/S2215-0366(23)00067-6

[5] Nguyen VV, Zainal NH, Newman MG. Why Sleep is Key: Poor Sleep Quality is a Mechanism for the Bidirectional Relationship between Major Depressive Disorder and Generalized Anxiety Disorder Across 18 Years. Journal of Anxiety Disorders. 2022; 90: 102601. https://doi.org/10.1016/j.janxdis.2022.102601

[6] Palagini L, Hertenstein E, Riemann D, Nissen C. Sleep, insomnia and mental health. Journal of Sleep Research. 2022; 31: e13628. https://doi.org/10.1111/jsr.13628

[7] Nguyen E, Meadley B, Harris R, Rajaratnam SMW, Williams B, Smith K, et al. Sleep and mental health in recruit paramedics: a 6-month longitudinal study. Sleep. 2023; 46: zsad050. https://doi.org/10.1093/sleep/zsad050

[8] Xiao T, Pan M, Xiao X, Liu Y. The relationship between physical activity and sleep disorders in adolescents: a chain-mediated model of anxiety and mobile phone dependence. BMC Psychology. 2024; 12: 751. https://doi.org/10.1186/s40359-024-02237-z

[9] Palmer CA, Alfano CA. Sleep and emotion regulation: An organizing, integrative review. Sleep Medicine Reviews. 2017; 31: 6–16. https://doi.org/10.1016/j.smrv.2015.12.006

[10] Palmer CA, Bower JL, Cho KW, Clementi MA, Lau S, Oosterhoff B, et al. Sleep loss and emotion: A systematic review and meta-analysis of over 50 years of experimental research. Psychological Bulletin. 2024; 150: 440–463. https://doi.org/10.1037/bul0000410

[11] Jackson ML, Sztendur EM, Diamond NT, Byles JE, Bruck D. Sleep difficulties and the development of depression and anxiety: a longitudinal study of young Australian women. Archives of Women's Mental Health. 2014; 17: 189–198. https://doi.org/10.1007/s00737-014-0417-8

[12] Buysse DJ, Angst J, Gamma A, Ajdacic V, Eich D, Rössler W. Prevalence, course, and comorbidity of insomnia and depression in young adults. Sleep. 2008; 31: 473–480. https://doi.org/10.1093/sleep/31.4.473

[13] Irwin MR. Why sleep is important for health: a psychoneuroimmunology perspective. Annual Review of Psychology. 2015; 66: 143–172. https://doi.org/10.1146/annurev-psych-010213-115205

[14] Akkaoui MA, Palagini L, Geoffroy PA. Sleep Immune Cross Talk and Insomnia. Advances in Experimental Medicine and Biology. 2023; 1411: 263–273. https://doi.org/10.1007/978-981-19-7376-5_12

[15] Vgontzas AN, Bixler EO, Lin HM, Prolo P, Mastorakos G, Vela-Bueno A, et al. Chronic insomnia is associated with nyctohemeral activation of the hypothalamic-pituitary-adrenal axis: clinical implications. The Journal of Clinical Endocrinology and Metabolism. 2001; 86: 3787–3794. https://doi.org/10.1210/jcem.86.8.7778

[16] Feng X, Jia M, Cai M, Zhu T, Hashimoto K, Yang JJ. Central-peripheral neuroimmune dynamics in psychological stress and depression: insights from current research. Molecular Psychiatry. 2025; 30: 4881–4898. https://doi.org/10.1038/s41380-025-03085-y

[17] Trzebanski S, Kim JS, Larossi N, Raanan A, Kancheva D, Bastos J, et al. Classical monocyte ontogeny dictates their functions and fates as tissue macrophages. Immunity. 2024; 57: 1225–1242.e6. https://doi.org/10.1016/j.immuni.2024.04.019

[18] Mitchell AJ, Roediger B, Weninger W. Monocyte homeostasis and the plasticity of inflammatory monocytes. Cellular Immunology. 2014; 291: 22–31. https://doi.org/10.1016/j.cellimm.2014.05.010

[19] Cluny NL, Nyuyki KD, Almishri W, Griffin L, Lee BH, Hirota SA, et al. Recruitment of α4β7 monocytes and neutrophils to the brain in experimental colitis is associated with elevated cytokines and anxiety-like behavior. Journal of Neuroinflammation. 2022; 19: 73. https://doi.org/10.1186/s12974-022-02431-z

[20] Niraula A, Witcher KG, Sheridan JF, Godbout JP. Interleukin-6 Induced by Social Stress Promotes a Unique Transcriptional Signature in the Monocytes That Facilitate Anxiety. Biological Psychiatry. 2019; 85: 679–689. https://doi.org/10.1016/j.biopsych.2018.09.030

[21] Liu G, Wang Y, Zheng W, Cheng H, Zhou R. P11 Loss-of-Function is Associated with Decreased Cell Proliferation and Neurobehavioral Disorders in Mice. International Journal of Biological Sciences. 2019; 15: 1383–1395. https://doi.org/10.7150/ijbs.33773

[22] Yue Y, Zhang J, Li Y, Ma X, Chen G, Zhu Z, et al. Disruptions of p11 (S100A10) and HPA Axis Homeostasis Participate in the Major Depressive Disorder (MDD) Especially in Female Patients. Neuropsychiatric Disease and Treatment. 2025; 21: 2237–2249. https://doi.org/10.2147/NDT.S549538

[23] Veldman ER, Mamula D, Jiang H, Tiger M, Ekman CJ, Lundberg J, et al. P11 (S100A10) as a potential predictor of ketamine response in patients with SSRI-resistant depression. Journal of Affective Disorders. 2021; 290: 240–244. https://doi.org/10.1016/j.jad.2021.04.055

[24] Svenningsson P, Berg L, Matthews D, Ionescu DF, Richards EM, Niciu MJ, et al. Preliminary evidence that early reduction in p11 levels in natural killer cells and monocytes predicts the likelihood of antidepressant response to chronic citalopram. Molecular Psychiatry. 2014; 19: 962–964. https://doi.org/10.1038/mp.2014.13

[25] Green H, Zhang X, Tiklova K, Volakakis N, Brodin L, Berg L, et al. Alterations of p11 in brain tissue and peripheral blood leukocytes in Parkinson's disease. Proceedings of the National Academy of Sciences of the United States of America. 2017; 114: 2735–2740. https://doi.org/10.1073/pnas.1621218114

[26] Cho WH, Noh K, Lee BH, Barcelon E, Jun SB, Park HY, et al. Hippocampal astrocytes modulate anxiety-like behavior. Nature Communications. 2022; 13: 6536. https://doi.org/10.1038/s41467-022-34201-z

[27] Wang J, Lu T, Gui Y, Zhang X, Cao X, Li Y, et al. HSPA12A controls cerebral lactate homeostasis to maintain hippocampal neurogenesis and mood stabilization. Translational Psychiatry. 2023; 13: 280. https://doi.org/10.1038/s41398-023-02573-5

[28] Le Faouder J, Arnaud B, Lavigne R, Lucas C, Com E, Bouvret E, et al. Fish Hydrolysate Supplementation Prevents Stress-Induced Dysregulation of Hippocampal Proteins Relative to Mitochondrial Metabolism and the Neuronal Network in Mice. Foods (Basel, Switzerland). 2022; 11: 1591. https://doi.org/10.3390/foods11111591

[29] Klinzing JG, Niethard N, Born J. Mechanisms of systems memory consolidation during sleep. Nature Neuroscience. 2019; 22: 1598–1610. https://doi.org/10.1038/s41593-019-0467-3

[30] Pronier É, Morici JF, Girardeau G. The role of the hippocampus in the consolidation of emotional memories during sleep. Trends in Neurosciences. 2023; 46: 912–925. https://doi.org/10.1016/j.tins.2023.08.003

[31] Li X, Kong Z, Cai K, Qi F, Zhu S. Neopterin mediates sleep deprivation-induced microglial activation resulting in neuronal damage by affecting YY1/HDAC1/TOP1/IL-6 signaling. Journal of Advanced Research. 2025; 72: 181–195. https://doi.org/10.1016/j.jare.2024.07.017

[32] Weerasinghe-Mudiyanselage PDE, Moon C. Recent Insights into Hippocampal Dysfunction and Neuroplasticity in Sleep Disorders: An Update from Preclinical Studies. Journal of Integrative Neuroscience. 2024; 23: 144. https://doi.org/10.31083/j.jin2308144

[33] Kotova MM, Amikishiev SV, Apukhtin KV, Galstyan DS, de Abreu MS, Stewart AM, et al. Prolonged 5-week and 12-week chronic stress differentially modulates CNS expression of pro- and anti-neuroinflammatory biomarkers, brain monoamines and affective behavior in adult zebrafish. Journal of Comparative Physiology. B, Biochemical, Systemic, and Environmental Physiology. 2025; 195: 305–321. https://doi.org/10.1007/s00360-025-01613-4

[34] Adavi H, Kowsar R, Radahmadi M, Alaei H. Comparing Various Types of Chronic Psychological Stress on Cognitive Functions and Behaviors in Rats. Basic and Clinical Neuroscience. 2024; 15: 301–316. https://doi.org/10.32598/bcn.2023.2346.4

[35] Hu X, Zhang L. The Central Role of Cytokines in PTSD and Major Depressive Disorder: Mechanisms and Clinical Implications. Immune Discovery. 2025; 1: 10013. https://doi.org/10.70322/immune.2025.10013

[36] Mancuso RA, Ross KM, Accortt E, Coussons-Read M, Okun ML, Irwin J, et al. Prenatal mood and anxiety disorders and associated cytokine changes. Journal of Affective Disorders. 2024; 347: 635–644. https://doi.org/10.1016/j.jad.2023.12.014

[37] Lee B, Kwon JT, Jeong Y, Caris H, Oh D, Feng M, et al. Inflammatory and anti-inflammatory cytokines bidirectionally modulate amygdala circuits regulating anxiety. Cell. 2025; 188: 2190–2202.e15. https://doi.org/10.1016/j.cell.2025.03.005

[38] HE L, Polisetty V, Nguyen T. The Immunopathogenesis of Autoimmune Encephalitis-Related Psychosis, A Comprehensive Review of Humoral and Cellular Mechanisms. Immune Discovery. 2025; 1: 10008. https://doi.org/10.70322/immune.2025.10008

[39] Wohleb ES, Powell ND, Godbout JP, Sheridan JF. Stress-Induced Recruitment of Bone Marrow-Derived Monocytes to the Brain Promotes Anxiety-Like Behavior. The Journal of Neuroscience: the official journal of the Society for Neuroscience. 2013; 33: 13820–13833. https://doi.org/10.1523/JNEUROSCI.1671-13.2013

[40] Guilliams M, Mildner A, Yona S. Developmental and Functional Heterogeneity of Monocytes. Immunity. 2018; 49: 595–613. https://doi.org/10.1016/j.immuni.2018.10.005

[41] Montgomery AB, Chen SY, Wang Y, Gadhvi G, Mayr MG, Cuda CM, et al. Tissue-resident, extravascular Ly6c^{-} monocytes are critical for inflammation in the synovium. Cell Reports. 2023; 42: 112513. https://doi.org/10.1016/j.celrep.2023.112513

[42] Liu Z, Wang H, Li Z, Dress RJ, Zhu Y, Zhang S, et al. Dendritic cell type 3 arises from Ly6C^{+} monocyte-dendritic cell progenitors. Immunity. 2023; 56: 1761–1777.e6. https://doi.org/10.1016/j.immuni.2023.07.001

[43] Lou Y, Han M, Liu H, Niu Y, Liang Y, Guo J, et al. Essential roles of S100A10 in Toll-like receptor signaling and immunity to infection. Cellular & Molecular Immunology. 2020; 17: 1053–1062. https://doi.org/10.1038/s41423-019-0278-1

[44] Liu H, Sun J, Wang Z, Han R, Zhao Y, Lou Y, et al. S100a10 deficiency in neutrophils aggravates ulcerative colitis in mice. International Immunopharmacology. 2024; 128: 111499. https://doi.org/10.1016/j.intimp.2024.111499

[45] Milosevic A, Liebmann T, Knudsen M, Schintu N, Svenningsson P, Greengard P. Cell- and region-specific expression of depression-related protein p11 (S100a10) in the brain. The Journal of Comparative Neurology. 2017; 525: 955–975. https://doi.org/10.1002/cne.24113

[46] Seo JS, Wei J, Qin L, Kim Y, Yan Z, Greengard P. Cellular and molecular basis for stress-induced depression. Molecular Psychiatry. 2017; 22: 1440–1447. https://doi.org/10.1038/mp.2016.118

[47] Dautan D, Camargo A, Branzell N, Brioschi VI, Doyon D, Covatta E, et al. Altered acetylcholine modulations and corticoaccumbal pathway in P11-linked social dysfunction. Molecular Psychiatry. 2026; 31: 1785–1798. https://doi.org/10.1038/s41380-025-03324-2

[48] Sun HL, Zhou ZQ, Zhang GF, Yang C, Wang XM, Shen JC, et al. Role of hippocampal p11 in the sustained antidepressant ef-

fect of ketamine in the chronic unpredictable mild stress model. Translational Psychiatry. 2016; 6: e741. https://doi.org/10.1038/tp.2016.21

[49] Seo JS, Zhong P, Liu A, Yan Z, Greengard P. Elevation of p11 in lateral habenula mediates depression-like behavior. Molecular Psychiatry. 2018; 23: 1113–1119. https://doi.org/10.1038/mp.2017.96

[50] Hanada Y, Kawahara Y, Ohnishi YN, Shuto T, Kuroiwa M, Sotogaku N, et al. p11 in Cholinergic Interneurons of the Nucleus Accumbens Is Essential for Dopamine Responses to Rewarding Stimuli. eneuro. 2018; 5: 318–332. https://doi.org/10.1523/ENEURO.0332-18.2018

[51] MacQueen G, Frodl T. The hippocampus in major depression: evidence for the convergence of the bench and bedside in psychiatric research? Molecular Psychiatry. 2011; 16: 252–264. https://doi.org/10.1038/mp.2010.80

[52] Elzinga SE, Guo K, Turfah A, Henn RE, Webber-Davis IF, Hayes JM, et al. Metabolic stress and age drive inflammation and cognitive decline in mice and humans. Alzheimer's & Dementia: the Journal of the Alzheimer's Association. 2025; 21: e70060. https://doi.org/10.1002/alz.70060

[53] Liu L, Zhou X, Zhang Y, Pu J, Yang L, Yuan S, et al. Hippocampal metabolic differences implicate distinctions between physical and psychological stress in four rat models of depression. Translational Psychiatry. 2018; 8: 4. https://doi.org/10.1038/s41398-017-0018-1

[54] Wu X, Ge H, Fang J, He J, Xu H, Zhao Y, et al. Sex-specific effects of maternal gestational diabetes mellitus on offspring neurodevelopment: persistent hippocampal neurogenesis deficits in female but not male offspring. Experimental & Molecular Medicine. 2026; 58: 1854–1869. https://doi.org/10.1038/s12276-026-01741-z

[55] Ong WY, Farooqui T, Koh HL, Farooqui AA, Ling EA. Protective effects of ginseng on neurological disorders. Frontiers in Aging Neuroscience. 2015; 7: 129. https://doi.org/10.3389/fnagi.2015.00129

[56] Wang Y, Zhang M, Li W. Targeting glial cells: Unveiling the neuroprotective mechanisms of Ginseng in the brain microenvironment. Acta Pharmaceutica Sinica. B. 2026; 16: 13–34. https://doi.org/10.1016/j.apsb.2025.10.018

[57] Zalachoras I, Hollis F, Ramos-Fernández E, Trovo L, Sonnay S, Geiser E, et al. Therapeutic potential of glutathione-enhancers in stress-related psychopathologies. Neuroscience and Biobehavioral Reviews. 2020; 114: 134–155. https://doi.org/10.1016/j.neubiorev.2020.03.015

[58] Ramanathan L, Siegel JM. Sleep deprivation under sustained hypoxia protects against oxidative stress. Free Radical Biology & Medicine. 2011; 51: 1842–1848. https://doi.org/10.1016/j.freeradbiomed.2011.08.016

[59] Zhang Y, Wu S, Tang W, Yang C, Yin Y, He J, et al. The Role of the Hippocampal P2X7R/NLRP3 Signaling Pathway in Depression-Like Behavior Induced by the Interaction Between Chronic Stress and Time in a Rat Model of Stroke. Journal of Integrative Neuroscience. 2025; 24: 40005. https://doi.org/10.31083/JIN40005

[60] Orihuela R, McPherson CA, Harry GJ. Microglial M1/M2 polarization and metabolic states. British Journal of Pharmacology. 2016; 173: 649–665. https://doi.org/10.1111/bph.13139

[61] Cao L, He C. Polarization of macrophages and microglia in inflammatory demyelination. Neuroscience Bulletin. 2013; 29: 189–198. https://doi.org/10.1007/s12264-013-1324-0

[62] Xue R, Wan Y, Sun X, Zhang X, Gao W, Wu W. Nicotinic Mitigation of Neuroinflammation and Oxidative Stress After Chronic Sleep Deprivation. Frontiers in Immunology. 2019; 10: 2546. https://doi.org/10.3389/fimmu.2019.02546

[63] Xie Y, Ba L, Wang M, Deng SY, Chen SM, Huang LF, et al. Chronic sleep fragmentation shares similar pathogenesis with neurodegenerative diseases: Endosome-autophagosome-lysosome pathway dysfunction and microglia-mediated neuroinflammation. CNS Neuroscience & Therapeutics. 2020; 26: 215–227. https://doi.org/10.1111/cns.13218

[64] Eguchi K. Phosphoinositides: Nanoscale Effects on Neuronal Membranes. The Neuroscientist: a Review Journal Bringing Neurobiology, Neurology and Psychiatry. 2025; 31: 576–590. https://doi.org/10.1177/10738584251337664

[65] Mehta K, Yentsch H, Lee J, Yook Y, Lee KY, Gao TT, et al. Phosphatidylinositol-3-phosphate mediates Arc capsid secretion through the multivesicular body pathway. Proceedings of the National Academy of Sciences of the United States of America. 2024; 121: e2322422121. https://doi.org/10.1073/pnas.2322422121

[66] Rivero-Ríos P, Uygun T, Chavis GD, Lee H, Duan B, Sutton MA, et al. PI(3)P coordinates SNX17- and SNX27-dependent protein recycling for long-term synaptic plasticity. The Journal of Cell Biology. 2025; 224: e202411198. https://doi.org/10.1083/jcb.202411198

[67] Guo Z, Jiang CH, Tong C, Yang Y, Wang Z, Lam SM, et al. Activity-dependent PI4P synthesis by PI4KIIIα regulates long-term synaptic potentiation. Cell Reports. 2022; 38: 110452. https://doi.org/10.1016/j.celrep.2022.110452

[68] Sang Y, Niu C, Xu J, Zhu T, You S, Wang J, et al. PI4KIIIβ-Mediated Phosphoinositides Metabolism Regulates Function of the VTA Dopaminergic Neurons and Depression-Like Behavior. The Journal of Neuroscience: the Official Journal of the Society for Neuroscience. 2024; 44: e0555232024. https://doi.org/10.1523/JNEUROSCI.0555-23.2024